Physics – Uspekhi **59** (10) 968 – 996 (2016)

REVIEWS OF TOPICAL PROBLEMS

PACS numbers: 03.65.Ta, 04.80.Na, **42.50. – p**

100th ANNIVERSARY OF THE BIRTH OF V L GINZBURG

Quantum measurements in gravitational-wave detectors

F Ya Khalili

DOI: https://doi.org/10.3367/UFNe.2016.07.037866

Contents

Abstract. The sensitivity of contemporary gravitational-wave detectors is so high that to a large extent it is limited by quantum fluctuations of light in them. Methods to suppress or evade these fluctuations are actively being developed, and the simplest of them, the injection of squeezed light, has already found application in the GEO600 detector. The aim of this review is first to acquaint the reader with the quantum mechanical limitations on the sensitivity of optomechanical devices in general and laser gravitational-wave detectors in particular and, second, to outline the methods for overcoming these limitations that are considered the most promising for implementation in current and planned detectors.

Keywords: gravitational-wave detectors, quantum noise, squeezed light, standard quantum limit, quantum nondemolition measurements, filter cavities, quantum speed meter, optical rigidity

1. Introduction

The 12th of January 2016 was the last day of the first observing run (O1) at two advanced LIGO (Laser Interferometer Gravitational-Wave Observatory) gravitational detectors, which started formally on 18 September 2015 but actually approximately two weeks earlier. During this run, gravitational-wave signals from black hole mergers were detected for the first time. Two signals were recorded, on 14 September 2015 [1] and 26 December 2015 [2].

This result was a great success for the General Relativity (GR) theory, which predicted the existence of gravitational waves already 100 years ago [3]. We note that in all previous known tests (Mercury perihelion shift, light beam deflection near the Sun, gravitational time dilation), GR was proved only for a nearly flat space–time, with gravitational potential values $\varphi \ll c^2$. There are a number of alternative gravity theories, which for relatively weak gravitational fields give the same results as GR does, and therefore correctly predict the mentioned effects. The change in the period of revolution of compact two-body systems (1993 Nobel Prize [4, 5]) was indirect proof of the existence of gravitational waves, but it did not change the situation because the orbital motion of such systems can be described well in the framework of the first post-Newtonian approximation (detailed discussions of this problem and many references can be found in reviews [6, 7]).

The first direct observation of gravitational waves also led to new discussions among astrophysicists [8, 9]. Subsequent observations of gravitational waves will obviously significantly change our interpretation of the Universe, as happened after the development of radio astronomy.

Finally, gravitational-wave detection was a colossal triumph for experimental physics. The measured value of dimensionless variation of the space–time metric h, which in the case of almost free masses in gravitational-wave detectors is a variation of the relative position between them, was of the order of 10^{-21}. With the length of LIGO interferometer arms

F Ya Khalili Lomonosov Moscow State University, Faculty of Physics, Leninskie gory 1, str. 2, 119991Moscow, Russian Federation
E-mail: khalili@phys.msu.ru

Received 8 June 2016
Uspekhi Fizicheskikh Nauk **186** (10) 1059 – 1089 (2016)
DOI: 10.3367/UFNr.2016.07.037866
Translated by A L Chekhov; edited by A M Semikhatov

$L = 4$ km, the corresponding absolute value of the offset is

$$x = \frac{hL}{2} \sim 10^{-18}\ m \tag{1.1}$$

(which is three orders of magnitude smaller than the size of the proton). The noise level in the frequency range 100–300 Hz with the highest sensitivity was lower than 10^{-23} $\mathrm{Hz}^{-1/2}$ in relative displacement units.

The road towards such incredibly high sensitivity took almost half a century of hard work by experimentalists around the world (see, e.g., reviews [10–13]). This journey started with J Weber's experiments; he was apparently the first to realize that the observation of gravitational waves from astrophysical sources is not an absolutely hopeless task [14]. As detectors, Weber used aluminum cylinders 1.5 m in length with a fundamental mode eigenfrequency of 1.7 kHz. In 1969, he reported the registration of gravitational waves, which was later proved to be an error. The signal level was $h \sim 10^{-16}$ [15], five orders larger than the signals detected at Advanced LIGO (ALIGO).

In the early 1970s, Weber's experiments were repeated by V B Braginsky's group at Moscow State University (MSU). Two solid-state detectors used by this group had parameters close to those of the Weber detectors, and their sensitivity was approximately the same. However, they did not succeed in detecting gravitational waves [16].

After that, a number of solid-state detectors were built around the world. In the 1980s, with the use of cryogenic temperatures and more sophisticated readout systems for mechanical oscillations, the sensitivity reached approximately $h \sim 10^{-18}$ [17]. After 2000, when the laser detector era had already begun, the sensitivity of solid-state detectors reached 10^{-21} $\mathrm{Hz}^{-1/2}$, but only in the narrow frequency band near mechanical resonance [18, 19]. However, none of these devices recorded gravitational waves.

These sensitivity values were already not too far from the level of quantum fluctuations in solid-state detectors, particularly, from the standard quantum limit (SQL), the characteristic limitation of measurement accuracy, which corresponds to the balance between the measurement error and a random back-action of the observer on the object due to the Heisenberg uncertainty principle.

This fact, together with the understanding that real gravitational-wave detection will require a sensitivity several orders of magnitude higher, stimulated the first work on the theory and methods of quantum measurements with macroscopic mechanical objects. Notably, at the end of the 1960s, Braginsky formulated the concept of the SQL [20, 21], and the first work describing measurement schemes that would allow overcoming this limit appeared in the 1970s [22–26]. Unfortunately, these studies did not receive direct experimental continuation, party due to the limited technologies of that time and mostly because the evolution of gravitational-wave detectors followed a radically different path, which involved laser interferometer detectors, which were suggested already in 1962 by Gertsenshtein and Pustovoit [27] (see also early review [10], where the authors emphasized the prospects of using optical measurement methods in gravitational-wave experiments).

It is interesting to note that almost 40 years later, these early studies appear to be in high demand in other fields of physics. Currently, a significant increase in interest is observed in the field of quantum optomechanical systems [28, 29]. The parameters of mechanical oscillators used in these experiments differ greatly from the vibrational modes of solid-state gravitational-wave detectors, but quantum measurement methods developed previously for the latter can be successfully applied to optomechanical systems. Such possibilities are being intensively discussed in the literature, and the first achievements have already been made in this field [30].

The first operating interferometer detector was built at the Hughes Research Laboratories in the late 1960s almost simultaneously with Weber's experiments [31]. Both the size and sensitivity of this detector were quite modest and could not compete with even the Weber detector. Later, in the 1980s, a number of so-called prototype interferometers were built around the world with arms several dozen meters long [32–34]. Their main purpose was not to detect gravitational waves but to work out the technologies that would be used in much larger devices in the future. However, their sensitivity could already be compared to those of the best solid-state detectors of that time, and exactly these interferometers were the first ones to reach a sensitivity level limited by quantum fluctuations of light.

Finally, in the 1990s, the construction of large laser interferometers began: LIGO [35, 36], Virgo [37], GEO 600 [38], and TAMA 300 [39]. The long arm lengths in these interferometers, from several hundred meters to several kilometers, from the very beginning gave them a radical advantage over solid-state detectors in terms of the sensitivity to a gravitational signal, even if the sensitivity to absolute displacement was the same [see Eqn (1.1)]. After several years of adjustments, in the mid-2000s, the LIGO detectors reached their planned sensitivity (record high at that time), which at the best point (around 150 Hz) exceeded $\sim 3 \times 10^{-23}$ $\mathrm{Hz}^{-1/2}$ [40]. This sensitivity was later slightly improved, in particular by using squeezed quantum states of light [41, 42].

A detailed history of laser gravitational-wave detectors can be found in review [19].

In 2011, the LIGO detectors were turned off for a radical upgrade. Actually, the only part left from the old interferometers was the shell–vacuum system: all other key elements were replaced with new ones. The planned sensitivity of the new ALIGO interferometers is one order of magnitude higher than that of the first-generation LIGO interferometers [43]. As a result, the first series of measurements using the new detectors, albeit with a slightly lower sensitivity than planned, was finally successful: gravitational waves were detected.

Large laser gravitational-wave detectors could be regarded as quantum devices already when they first appeared. Even in first-generation detectors, a significant part of the operating frequency range, approximately 200 Hz and higher, was limited by quantum fluctuations of the light phase (shot noise). At lower frequencies, various technological noises were dominant, including seismic noise and thermal noise of mirror suspensions (a detailed characterization of noises at the LIGO detectors is given in Fig. 7 in [40]). These noises will be significantly decreased in second-generation detectors, and the dominant noise at lower frequencies will be the radiation pressure noise, which corresponds to the displacement of the detector test mirrors caused by fluctuations of the radiation pressure force acting on them, which, in turn, are created by quantum fluctuations of light power in the interferometer arms. At the best sensitivity point (around 100 Hz for ALIGO), the levels of shot noise and radiation pressure noise will be approximately the same, and their sum will be equal to the SQL. For the ALIGO parameters [see Eqns (3.42a)–(3.42d)], this corresponds to a sensitivity of

Table 1. Main notations used in this review.

c	Speed of light
h	Dimensionless gravitational-wave signal (metric variation)
$\hbar$	Planck constant
I_0	Pump laser power
I_c	Total optical power in two interferometer arms
$\mathcal{K}(\Omega)$	Optomechanical coupling coefficient for the Michelson/Fabry–Perot interferometer [see Eqn (3.37)]
$\mathcal{K}_{SM}(\Omega)$	Optomechanical coupling coefficient for the Sagnac/Fabry–Perot interferometer [see Eqn (4.61)]
L	Length of interferometer arms
m	Test object mass; reduced mass of interferometer mirrors
M	Physical mass of interferometer mirrors
Q_m	Quality factor of a mechanical oscillator
e^r	Amplitude squeezing factor; r is a dimensionless parameter that characterizes the squeezing rate on a logarithmic scale
γ	FWHM of the optical cavity transmission band
δ	Optical pump frequency detuning from the optical cavity eigenfrequency
ϵ^2	Normalized optical losses in the interferometer [see Eqn (4.7)]
ζ	Homodyne phase
η	Unified quantum efficiency of the interferometer
Θ	Normalized optical power [see Eqn (3.38)]
θ	Squeezing phase
Ω	Any low (mechanical) frequency
Ω_m	Mechanical oscillator eigenfrequency
ω	Any high (optical) frequency
ω_0	Optical cavity eigenfrequency

approximately 2×10^{-24} $\mathrm{Hz}^{-1/2}$ [see Eqn (2.28)], almost on the level of the planned sensitivity of these detectors and not so far from the result already demonstrated by them.

According to reasonably optimistic astrophysical predictions, detectors with such sensitivity should be able to record several gravitational-wave signals every year [44]. However, in order to transform gravitational-wave detectors into a regular source of astrophysical data, their sensitivity must be increased by one order of magnitude at least. This means that the situation that took place in the 1970s is repeated at another stage: currently planned third-generation detectors would most probably require quantum measurement schemes that would overcome the SQL.

In this review, we analyze the quantum limitations of sensitivity in laser gravitational-wave detectors, together with methods that can help to overcome these limitations and are currently considered to be the most promising.

In Section 2, we describe the main principles of the theory of linear quantum probe systems, which is the basis of methods for analyzing quantum noises in gravitational-wave detectors. Section 3 is devoted to quantum noises in laser interferometers, and in Section 4 we discuss some methods for suppressing these noises, both already applied and planned to be used in future detectors.

The notation used in this review is summarized in Table 1.

We try to avoid cumbersome mathematical calculations by using simplified models and qualitative physical considerations whenever possible. Those readers who would like to study the applications of quantum measurement theory to laser gravitational-wave detectors in more detail are referred to the significantly larger and thorough review [45].

2. Basic principles

2.1 Linear quantum probe system

When analyzing the quantum limitations in gravitational-wave detectors, two facts play a key role. First, the energy flux in gravitational waves from astrophysical sources is not small and corresponds to a huge number of gravitons [46]. For example, in a signal registered on 14 September 2015, it was approximately 0.3 mJ m^{-2}; there is no problem registering an electromagnetic pulse with the same energy. All problems arise due to an extremely weak interaction of gravitational waves with matter. On the other hand, this fact allows fully neglecting back-action of the detector on the gravitational wave and describe the action of the latter with a classical (deterministic) force.

Second, the weakness of both this force and the principal noise sources in gravitational-wave detectors allows linearizing equations of motion with high accuracy in the vicinity of a chosen operation point.

This means that gravitational-wave detectors can be considered a *linear quantum probe system* [47–49] with the equivalent schematic shown in Fig. 1. A classical force $F_{sign}(t)$, which has to be detected, acts on a quantum test object, for example, on a vibrational mode of a solid-state bar detector or on some joint motion mode of interferometer mirrors. The test object coordinate $\hat{x}$ is measured by a *linear quantum meter*, which returns the sum

$$\tilde{x}(t) = \hat{x}(t) + \hat{x}_{fl}(t)\,, \tag{2.1}$$

where $\hat{x}_{fl}$ is the *measurement noise* (here and hereafter, we use the Heisenberg representation, which is standard when considering such systems). Due to the Heisenberg uncertainty principle, a coordinate measurement is always followed by a perturbation of the corresponding canonically

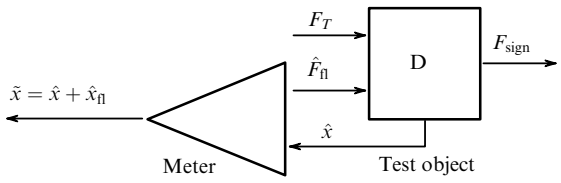

Figure 1. Equivalent schematic of a linear quantum probe system.

conjugate momentum. The physical source of such a perturbation is a random force, so-called *back-action noise* $\hat{F}_{\rm fl}$, with which the meter acts on the test object.

Moreover, the test object can be influenced by various other noise forces of a 'technological' nature, denoted in Fig. 1 by F_T. In Section 2, we consider the most fundamental of them, the thermal noise corresponding to friction in the test object.

The existence of noises $\hat{x}_{\rm fl}$ and $\hat{F}_{\rm fl}$ follows from basic principles of quantum theory. This is connected with the fact that values of the test object coordinate operator at different time instants do not commute in general because they cannot be measured simultaneously:

$$\left[\hat{x}(t), \hat{x}(t')\right] \neq 0\,. \tag{2.2}$$

But the output signal of the meter is a classical observable, for which continuous precise measurement is possible, and therefore

$$\left[\tilde{x}(t), \tilde{x}(t')\right] \equiv 0\,. \tag{2.3}$$

As was shown in [49], this contradiction can be resolved by modifying the test object evolution with the back-action noise and adding measurement noise to the output signal.

The general relations that must be satisfied by these noises are quite complicated [47, 48]. Here, we consider them in a particular case of stationary noises (those invariant under time shifts) because this is the case of modern gravitational-wave detectors, whose parameters can be considered constant (up to an undesirable slow drift due to various external factors).

Stationary noises can be characterized by their spectral densities, which depend on the observation frequency Ω in general. Spectral densities of measurement noise S_x, fluctuation back-action noise S_F, and their cross-spectral density (cross-correlation) S_{xF} satisfy the following inequality, which has the form (and physical meaning) of the standard Schrödinger–Robertson uncertainty relation:

$$S_x(\Omega)S_F(\Omega) - \left|S_{xF}(\Omega)\right|^2 \geqslant \frac{\hbar^2}{4} \tag{2.4}$$

[here and hereafter, unless stipulated otherwise, we use the so-called double-sided definition of the spectral density (see Appendix A)].

The physical sources of noises $x_{\rm fl}$ and $F_{\rm fl}$ in laser interferometers are the fluctuations of phase and amplitude of light in them. Because the energies of optical quanta correspond to temperatures of several dozen thousand degrees, we can disregard thermal noises and still maintain high accuracy (thermal noises must not be confused with mechanical thermal noises of test masses!). Excess technological noises of the pump laser in gravitational-wave detectors are suppressed due to the interferometer geometry and the use of feedback systems (see more details in Section 3.1). Therefore, optical noises in laser gravitational-wave detectors can be considered purely quantum, which results in the strict equality in relation (2.4). Explicit expressions for these noises are given in Sections 3 and 4 for different types of interferometers.

2.2 Total quantum noise

2.2.1 General case. We return to the schematic in Fig. 1. Its general evolution is defined by the input/output relation for quantum meter (2.1) and by the equation of motion of the test object

$$\mathrm{D}\left[\hat{x}(t)\right] = F_{\rm sign}(t) + \hat{F}_{\rm fl}(t) + F_T(t)\,, \tag{2.5}$$

where D is the differential operator that describes the test object dynamics: $\mathrm{D} = -m\,\mathrm{d}^2/\mathrm{d}t^2$ for a free mass and $\mathrm{D} = m(-\mathrm{d}^2/\mathrm{d}t^2 + \Omega_0^2)$ for a harmonic oscillator.

Substituting the solution of Eqn (2.5) in expression (2.1), we obtain

$$\tilde{x}(t) = \hat{x}_0(t) + \mathrm{D}^{-1}\left[F_{\rm sign}(t) + \hat{F}_{\rm fl}(t) + F_T(t)\right] + \hat{x}_{\rm fl}(t)\,, \tag{2.6}$$

where $x_0(t)$ is the eigenmotion of the test object and D^{-1} is the integral operator that is the inverse of D. In particular, for a free mass m,

$$\hat{x}_0(t) = \hat{x} + \frac{\hat{p}t}{m}\,, \tag{2.7}$$

$$\mathrm{D}^{-1}\left[F(t)\right] = \frac{1}{m}\int_0^\infty (t - t')\,F(t')\,\mathrm{d}t'\,, \tag{2.8}$$

where $\hat{x}$ and $\hat{p}$ are coordinate and momentum operators in the Schrödinger representation ('initial conditions').

Equation (2.6) can be written in the equivalent form

$$\tilde{x}(t) = \hat{x}_0(t) + \mathrm{D}^{-1}\left[F_{\rm sign}(t) + \hat{F}_{\rm tot}(t) + F_T(t)\right]\,, \tag{2.9}$$

where

$$\hat{F}_{\rm tot}(t) = \mathrm{D}\left[\hat{x}_{\rm fl}(t)\right] + \hat{F}_{\rm fl}(t) \tag{2.10}$$

is the *total quantum noise* of the meter.

2.2.2 Test object quantization. Based on the obtained relations, we can conclude that there are the following contributions to the quantum uncertainties of the meter output signal: the initial quantum state of the test object (the term $\hat{x}_0$) and the noises $\hat{x}_{\rm fl}$ and $\hat{F}_{\rm fl}$ of the meter. It may seem that both these factors limit the sensitivity of the linear quantum probe system. This conclusion is false, however; the contribution of the probe object initial state is eliminated by a trivial linear transformation of the meter output signal [49]. Indeed, for any linear system,

$$\mathrm{D}\left[\hat{x}_0(t)\right] \equiv 0\,. \tag{2.11}$$

Therefore, the action of the operator D on $\tilde{x}$ is expressed as

$$\tilde{F}_{\rm sign}(t) = \mathrm{D}\left[\tilde{x}(t)\right] = F_{\rm sign}(t) + \hat{F}_{\rm tot}(t) + F_T(t)\,, \tag{2.12}$$

where $\tilde{F}_{\rm sign}$ is the signal force estimate.

Thus, we have come to an important conclusion: in linear quantum probe systems, the initial quantum state of the test object itself does not matter. The only source of quantum limitations of the sensitivity is the meter, which in the case of laser gravitational-wave detectors is quantum fluctuations of light in it.

2.2.3 Spectral density of the total quantum noise. We consider the special case of a stationary quantum probe system in more detail. In such a system, (a) quantum noises are stationary and (b) the dynamics are also stationary (i.e., the parameters of the test object do not depend on time); the importance of this case was already mentioned before. It is therefore reasonable to use the spectral representation, in which the total quantum

noise in (2.10) has the form

$$\hat{F}_{\rm tot}(\Omega) = \chi^{-1}(\Omega)\hat{x}_{\rm fl}(\Omega) + \hat{F}_{\rm fl}(\Omega)\,, \tag{2.13}$$

where $\chi(\Omega)$ is the generalized test-object susceptibility function, that is, the Fourier transform of the operator D^{-1} (also see our notational conventions in Appendix A). The spectral density of this noise then has the form

$$S_{\rm tot}(\Omega) = \left|\chi^{-1}(\Omega)\right|^2 S_x(\Omega) + 2\,\mathrm{Re}\left[\chi^{-1}(\Omega)S_{xF}(\Omega)\right] + S_F(\Omega)\,. \tag{2.14}$$

Usually, when analyzing the gravitational-wave detector sensitivity, the spectral densities are normalized not to the signal force, as in Eqn (2.14) (F-normalization), but to the dimensionless gravitational-wave signal h (h-normalization). We use the superscript h to denote such spectral densities. The relation between $F_{\rm sign}$ and h is described by the known relation (3.25) (see Section 3.1.4). In addition, the so-called one-sided definition of the spectral density is traditionally used for S^h, which gives values twice as large (see Appendix A). As a result, the expression for the total quantum noise spectral density in the h-normalization takes the form [see Eqn (A.4)]

$$S^h_{\rm tot}(\Omega) = \frac{8}{m^2L^2\Omega^4}\left\{\left|\chi^{-1}(\Omega)\right|^2 S_x(\Omega) + 2\,\mathrm{Re}\left[\chi^{-1}(\Omega)S_{xF}(\Omega)\right] + S_F(\Omega)\right\}. \tag{2.15}$$

2.3 Standard quantum limit

2.3.1 General case. The structure of expression (2.10) for the total quantum noise, which includes two terms that are connected through uncertainty relation (2.4), allows assuming that there is some optimal situation where the contributions of the measurement and back-action noises are equal and the probe system reaches its fundamental sensitivity limit — the standard quantum limit mentioned above. As we see below, this conclusion is false in the general case. However, there is an important subclass of quantum probe systems in which the SQL is indeed attained; this subclass is already important because all currently operating gravitational-wave detectors belong to it.

We assume that (a) the probe system is stationary and (b) its measurement noise and back-action noise do not correlate:

$$S_{xF} = 0\,. \tag{2.16}$$

The second assumption corresponds to the so-called *classical optimization* of the measurement noise $x_{\rm fl}$. In laser interferometers, classical optimization provides a minimal value of measurement noise for a given optical power, which has the best result when the measurement accuracy is not too high and measurement noise dominates the back-action noise (see more details in Section 3.3).

In this case, the spectral density of the total quantum noise takes the form

$$S_{\rm tot}(\Omega) = \left|\chi^{-1}(\Omega)\right|^2 S_x(\Omega) + S_F(\Omega)\,, \tag{2.17}$$

and the spectral densities S_x and S_F in (2.17) turn out to be connected through the 'simplified' uncertainty relation

$$S_x(\Omega)S_F(\Omega) \geqslant \frac{\hbar^2}{4}\,. \tag{2.18}$$

It is easy to see that if quantum noises are small enough to satisfy the exact equality in (2.18) and the condition

$$\frac{S_F(\Omega)}{S_x(\Omega)} = \left|\chi^{-1}(\Omega)\right|^2 \tag{2.19}$$

is satisfied, then the spectral density reaches its minimum:

$$S_{\rm SQL}(\Omega) = \hbar\left|\chi^{-1}(\Omega)\right|. \tag{2.20}$$

The last expression is the general case of the SQL spectral form.

We also write relations (2.17) and (2.20) in the h-normalization:

$$S^h_{\rm tot}(\Omega) = \frac{8\hbar}{m^2L^2\Omega^4}\left[\left|\chi^{-1}(\Omega)\right|^2 S_x(\Omega) + S_F(\Omega)\right], \tag{2.21}$$

$$S^h_{\rm SQL}(\Omega) = \frac{8\hbar}{m^2L^2\Omega^4}\left|\chi^{-1}(\Omega)\right|. \tag{2.22}$$

Importantly, for sensitivity (2.20) to be attained in some frequency band, relation (2.19) must be satisfied over the whole band. However, the frequency dependences of the spectral densities $S_x(\Omega)$ and $S_F(\Omega)$ in 'conventional' interferometers [see Eqns (3.39a–c)] do not correspond to the frequency dependence of the generalized susceptibility $\chi(\Omega)$ for real test objects (free mass and oscillator). In such cases, relation (2.20) is satisfied only at one or several frequencies; at other frequencies, the spectral density $S_{\rm SQL}$ is strictly greater than the SQL.

We consider practically important cases of a free test mass and a test oscillator in more detail. For simplicity, we assume that the spectral densities S_x and S_F are frequency-independent. This assumption is quite realistic and corresponds to the case where the considered frequency band belongs to the transmission band of the interferometer.

2.3.2 Free mass. The generalized susceptibility of a free mass has the form [1]

$$\chi(\Omega) = -\frac{1}{m\Omega^2}\,. \tag{2.23}$$

Hence,

$$S_{\rm tot}(\Omega) = m^2\Omega^4 S_x + S_F = \frac{\hbar m\Omega^2}{2}\left(\frac{\Omega^2}{\Omega_{\rm q}^2} + \frac{\Omega_{\rm q}^2}{\Omega^2}\right), \tag{2.24}$$

where

$$\Omega_{\rm q} = \left(\frac{S_F}{m^2 S_x}\right)^{1/4} \tag{2.25}$$

is the meter parameter characterizing the strength of its interaction with the test object. In laser interferometers, $\Omega_{\rm q}^2$ is proportional to the optical power [see Eqn (3.41)]. In the case of a free test mass, $\Omega_{\rm q}$ also defines the threshold frequency at which the contributions of measurement noise and back-action noise become equal and $S_{\rm tot}$ reaches the

[1] We ignore the effect of friction on the free mass dynamics, because it becomes visible only at very low frequencies, for which various nonquantum noises become dominant.

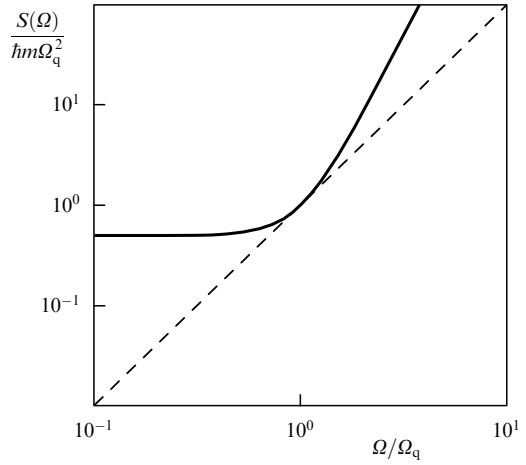

Figure 2. Total quantum noise (solid curve) and the SQL (dashed line) for a free mass, normalized to the signal force $F_{\rm sign}$.

SQL:

$$S_{\rm SQL}(\Omega) = \hbar m\Omega^2 \,. \tag{2.26}$$

The back-action noise dominates at lower frequencies, and the measurement noise, at higher frequencies; in both cases, $S_{\rm tot} > S_{\rm SQL}$. Figure 2 shows the dependences of $S_{\rm tot}$ and $S_{\rm SQL}$ that illustrate these relations.

In the h-normalization, Eqns (2.24) and (2.26) take the form

$$S^h_{\rm tot}(\Omega) = \frac{S^h_{\rm SQL}(\Omega)}{2}\left(\frac{\Omega^2}{\Omega_q^2} + \frac{\Omega_q^2}{\Omega^2}\right), \tag{2.27}$$

$$S^h_{\rm SQL}(\Omega) = \frac{8\hbar}{mL^2\Omega^2} \,. \tag{2.28}$$

These spectral densities are plotted in Fig. 3.

2.3.3 Harmonic oscillator. The generalized susceptibility of the harmonic oscillator has the form

$$\chi(\Omega) = \frac{1}{m(-\Omega^2 - {\rm i}\Omega\Omega_{\rm m}/Q_{\rm m} + \Omega_{\rm m}^2)} \,, \tag{2.29}$$

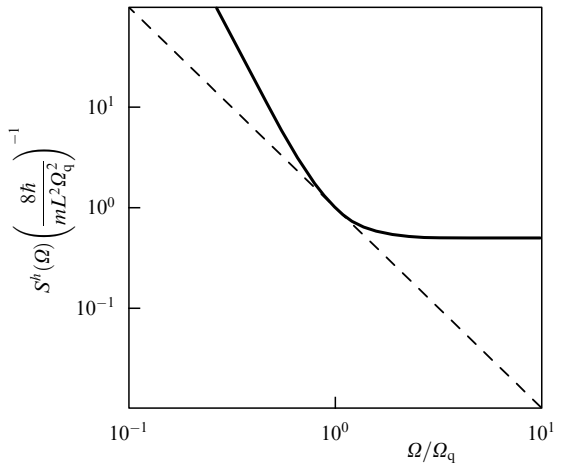

Figure 3. Total quantum noise (solid curve) and the SQL (dashed line) for a free mass, normalized to the gravitational-wave signal h.

which gives the following expressions for the total quantum noise and the SQL

$$S_{\rm tot}(\Omega) = m^2\left[(\Omega_{\rm m}^2 - \Omega^2)^2 + \frac{\Omega^2\Omega_{\rm m}^2}{Q_{\rm m}^2}\right]S_x + S_F \,, \tag{2.30}$$

$$S_{\rm SQL}(\Omega) = \hbar m\left[(\Omega_{\rm m}^2 - \Omega^2)^2 + \frac{\Omega^2\Omega_{\rm m}^2}{Q_{\rm m}^2}\right]^{1/2} . \tag{2.31}$$

We can clearly see from these expressions that the existence of a resonant maximum in the generalized susceptibility of a harmonic oscillator leads to the suppression of the measurement noise contribution and hence to a decrease in the SQL in the vicinity of the resonance frequency $\Omega_{\rm m}$.

Taking this into account, we consider the frequency band near $\Omega_{\rm m}$, assuming that

$$|\Omega - \Omega_{\rm m}| \ll \Omega_{\rm m} \,. \tag{2.32}$$

Assumption (2.32) allows simplifying relations (2.30) and (2.31):

$$S_{\rm tot}(\Omega) = \frac{\hbar m}{2}\left[\frac{4\Omega_{\rm m}^2(v^2 + \Gamma_{\rm m}^2)}{\Omega_q^2} + \Omega_q^2\right], \tag{2.33}$$

$$S_{\rm SQL}(\Omega) = 2\hbar m\Omega_{\rm m}\sqrt{v^2 + \Gamma_{\rm m}^2} \,, \tag{2.34}$$

where $v = \Omega - \Omega_{\rm m}$ is the detuning from the resonance frequency and $\Gamma_{\rm m} = \Omega_{\rm m}/(2Q_{\rm m})$ is the oscillator damping rate.

It follows from Eqn (2.33) that the smaller $\Omega_{\rm q}$ (the *less accurate* the measurement), the *better is the sensitivity* of the harmonic oscillator in the vicinity of its resonance frequency. This paradox can be explained easily: near the resonance frequency, back-action noise becomes dominant in the total quantum noise (2.33) and decreases as the measurement accuracy decreases. However, this advantage can be used only by narrowing the frequency band $\Delta\Omega$ where it takes place. In the limit case where

$$\Omega_q = \sqrt{2\Omega_{\rm m}\Gamma_{\rm m}} = \frac{\Omega_{\rm m}}{\sqrt{Q_{\rm m}}} \,, \tag{2.35}$$

the total quantum noise spectral density of a harmonic oscillator

$$S_{\rm tot}(\Omega) = \hbar m\Omega_{\rm m}\left(\frac{v^2}{\Gamma_{\rm m}} + 2\Gamma_{\rm m}\right) \tag{2.36}$$

is approximately $Q_{\rm m}$ times smaller that for a free mass, but only in a very narrow frequency range $\sim \Gamma_{\rm m}$.

This case is highly hypothetical, however. It is known that due to inherent Brownian fluctuations of the test object, the level of quantum noise can be reached under real experimental conditions only if the measurement time is small compared with its damping time [50], in other words, if the frequency band $\Delta\Omega \gg \Gamma_{\rm m}$ (see also Section 2.4). In this case, expressions (2.33) and (2.34) are simplified to

$$S_{\rm tot}(\Omega) = \frac{\hbar m}{2}\left(\frac{4\Omega_{\rm m}^2 v^2}{\Omega_q^2} + \Omega_q^2\right) = \frac{\hbar m\Omega_{\rm m}}{2}\left(\frac{4v^2}{\Delta\Omega} + \Delta\Omega\right), \tag{2.37}$$

$$S_{\rm SQL}(\Omega) = 2\hbar m\Omega_{\rm m}|v| \,, \tag{2.38}$$

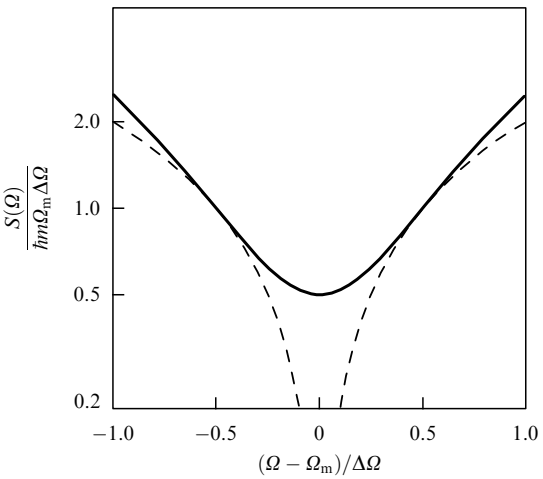

Figure 4. Total quantum noise (solid line) and the SQL (dashed line) for an oscillator, normalized to the signal force F_{sign}. (Logarithmic scale on the y axis.)

where

$$\Delta\Omega = \sqrt{\Omega_m \Omega_q} \tag{2.39}$$

is the transmission band defined in a conventional way 'by the $\sqrt{2}$ level', such that

$$S_{tot}\left(\Omega_m \pm \frac{\Delta\Omega}{2}\right) = 2S_{tot}(\Omega_m)\,. \tag{2.40}$$

Spectral densities (2.37) and (2.38) are plotted in Fig. 4.

By comparing (2.26) and (2.38), we can see that the test oscillator improves the quantum noise spectral density by a factor of $\Omega_m/\Delta\Omega$ compared to the case of a free mass.

In concluding this section, we recall that all sensitivity limitations obtained here hold only for certain quantum meters that satisfy the assumptions made above. As shown in Section 2.5, for a 'correct' quantum noise optimization, the sensitivity can be significantly higher, but to date this possibility has remained hypothetical and the obtained relations are still important.

2.4 Condition of the test object quantumness

Obviously, in order to reach the quantum level of sensitivity, all nonquantum noise sources must to be suppressed to a level lower than the quantum noise level. In real experiments, many different noise sources must be taken into account (a review of main noise sources in ALIGO detectors can be found in [43]). In many cases, particularly in solid-state gravitational-wave detectors and modern 'table-top' quantum optomechanical experiments, the leading contribution is made by thermal (Brownian) fluctuations of the test object center of mass. After many years of work, experimentalists succeeded in significantly suppressing this noise in laser gravitational-wave detectors, but it still has great influence at very low frequencies. In any case, the requirements applied to this noise are an important *necessary* condition for the quantum sensitivity to be reachable.

We return to expression (2.12) for the output signal of the quantum probe system. In view of the foregoing, we assume that the 'technological' noise F_T, which is one of the terms, is thermal noise with the spectral density

$$S_T = 2\kappa_B T H\,, \tag{2.41}$$

where κ_B is the Boltzmann constant, H is the coefficient of friction in the test object, and T is its temperature.[2]

Obviously, the necessary condition for the SQL to be reachable is the validity of the inequality

$$S_T < S_{SQL}\,, \tag{2.42}$$

and the use of any methods to overcome the SQL (to be discussed in Section 4) must be accompanied by a proportional suppression of thermal noise. From this standpoint, condition (2.42), which was first mentioned in [50], is a 'gateway' to the quantum world.

Substituting expressions (2.26) and (2.38) in inequality (2.42) and taking (2.41) into account, we can transform (2.42) into the following requirement for the test body temperature:

$$T < T_q\,, \tag{2.43}$$

where

$$T_q = \frac{\hbar m\Omega^2}{2\kappa_B H} \tag{2.44}$$

is the 'quantum temperature' for a free mass and

$$T_q = \frac{\hbar m\Omega_m\Delta\Omega}{2\kappa_B H} \tag{2.45}$$

for a harmonic oscillator, where $\Delta\Omega$ is the signal frequency band centered at Ω_m.

Generally speaking, the friction coefficient H depends on the observation frequency Ω. This dependence barely matters in test oscillators, because the operating frequencies in them are usually close to the resonance frequency Ω_m and the friction coefficient can be approximated as

$$H(\Omega) \approx H(\Omega_m) = \frac{m\Omega_m}{Q_m}\,. \tag{2.46}$$

At the same time, the so-called free masses that are used in laser gravitational-wave detectors are actually low-frequency pendulums with eigenfrequencies of the order of 1 Hz, while the operating band of such detectors starts approximately at 10 Hz and higher. Losses in high-quality silica suspensions of these pendulums can be approximated using the so-called structure friction model [52], according to which the friction coefficient is inversely proportional to the frequency:

$$H(\Omega) = \frac{\Omega_m}{\Omega}\,H(\Omega_m) = \frac{m\Omega_m^2}{\Omega Q_m}\,. \tag{2.47}$$

Hence, Eqns (2.44) and (2.45) can be written as

$$T_q = \frac{\hbar Q_m \Omega^3}{2\kappa_B \Omega_m^2}\,, \tag{2.48}$$

for 'almost free test masses', where Ω is the observation frequency, and as

$$T_q = \frac{\hbar Q_m \Delta\Omega}{2\kappa_B} \tag{2.49}$$

for test oscillators.

[2] We assume that $\kappa_B T \gg \hbar\Omega$. This assumption is valid with high precision for almost all mechanical objects used in modern experiments, including test masses of gravitational-wave detectors, except only exotic cryogenic mechanical oscillators in the gigahertz band [51], for which T should be replaced by $\hbar\Omega/(2\kappa_B)\coth(\hbar\Omega/(2\kappa_B T))$.

Interestingly, the quantumness condition (2.49) for an oscillator was obtained in [53, 54] based on completely different considerations, that is, the requirement for the quantum state decoherence time to be not less than some specified value $\tau_{\rm decoh} \sim 1/\Delta\Omega$.

We estimate the validity of condition (2.43) for gravitational-wave detectors. As an example, we consider the ultracryogenic resonant-bar gravitational-wave detector AURIGA (in Italian Antenna Ultracriogenica Risonante per l'Indagine Gravitazionale Astronomica) [19] with the best $Q_{\rm m}/T$ ratio. Its resonance frequency is close to the value typical for such detectors, 1 kHz, and $Q_{\rm m} = 3 \times 10^6$, which gives the value

$$T_{\rm q} \approx 0.07\,\frac{\Delta\Omega}{\Omega_{\rm m}}\ [{\rm K}]\,, \tag{2.50}$$

which is significantly (but not hopelessly) smaller than the real operating temperature $T = 0.25$ K.

To estimate the amount of this type of noise in laser detectors, we use the results in [55], where a record-high quality factor $Q_{\rm m} \approx 1.7 \times 10^8$ s (at room temperature) was obtained for a low-frequency oscillator with the eigenfrequency $f_{\rm m} \approx 0.3$ Hz (a prototype of laser gravitational-wave detector test masses). Using expression (2.48), we obtain the quantum temperature for such a test object:

$$T_{\rm q} \approx 5 \times 10^4 \left(\frac{\Omega}{2\pi \times 100\ {\rm Hz}}\right)^3\ [{\rm K}]\,. \tag{2.51}$$

This means that for characteristic times of the order of the gravitational wave period, the translational degrees of freedom of the laser gravitational-wave detector mirror center of mass can be regarded as quantum objects even at room temperature.

Unfortunately, in interferometers, light interacts not with the center of mass of the mirrors, but with their surfaces. In comparison with the motion of the center of mass, the motion of the surface includes a large number of noises [56]. In modern gravitational-wave detectors, the most serious problem is the Brownian fluctuations of the thickness of the reflective dielectric coating of the mirrors [43]. Decreasing the level of these noises is one of the main tasks for future detectors [57, 58].

2.5 Sensitivity limit for coordinate measurements

Methods for overcoming the SQL that are now regarded as candidates for realization in future laser gravitational-wave detectors are based on using (a) the cross-correlation of measurement noise and back-action noise and (b) specially tailored frequency dependences of the spectral densities of these noises, without giving up the stationarity assumption. This approach was first suggested in [59] and the sensitivity limit of this method was calculated in papers [60, 61] (for the general case of a linear quantum probe system) and in [62] (for the special case of an optical interferometer).

Here, we present a simplified version of the analysis in [60] assuming that

$$\operatorname{Im} S_{xF} = 0\,. \tag{2.52}$$

Assumption (2.52) significantly simplifies the calculations and at the same time gives the correct final result. It holds for laser interferometers if the pump frequency equals the interferometer resonance frequency ω_0. It is known that the detuning regime provides some interesting opportunities, which we discuss in Section 4.4, but their application is not planned in detectors currently being developed.

With assumption (2.52), the total quantum noise spectral density (2.13) takes the form

$$S_{\rm tot}(\Omega) = \left|\chi^{-1}(\Omega)\right|^2 S_x(\Omega) + 2\operatorname{Re}\chi^{-1}(\Omega)\,S_{xF}(\Omega) + S_F(\Omega)\,. \tag{2.53}$$

Just as we did in deriving the SQL, we assume that the exact equality holds in (2.4). Combining (2.4) and (2.53), we then obtain

$$S_{\rm tot}(\Omega) = \left|\chi^{-1}(\Omega)\right|^2 \frac{\hbar^2/4 + S_{xF}^2(\Omega)}{S_F(\Omega)} + 2\operatorname{Re}\chi^{-1}(\Omega)\,S_{xF}(\Omega) + S_F(\Omega)\,. \tag{2.54}$$

With

$$S_{xF}(\Omega) = -\frac{\operatorname{Re}\chi^{-1}(\Omega)}{\left|\chi^{-1}(\Omega)\right|^2}\,S_F(\Omega)\,, \tag{2.55}$$

spectral density (2.54) reaches its minimum with respect to $S_{xF}(\Omega)$:

$$S_{\rm tot}(\Omega) = \frac{\hbar^2\left|\chi^{-1}(\Omega)\right|^2}{4S_F(\Omega)} + \frac{\left[\operatorname{Im}\chi^{-1}(\Omega)\right]^2}{\left|\chi^{-1}(\Omega)\right|^2}\,S_F(\Omega)\,. \tag{2.56}$$

In turn, the last expression reaches its minimum with respect to $S_F(\Omega)$ when

$$S_F(\Omega) = \frac{\hbar}{2}\,\frac{\left|\chi^{-1}(\Omega)\right|^2}{\left|\operatorname{Im}\chi^{-1}(\Omega)\right|}\,, \tag{2.57a}$$

which gives the following expressions for S_x, S_{xF}, and the optimized spectral density of the total quantum noise:

$$S_x(\Omega) = \frac{\hbar}{2\left|\operatorname{Im}\chi^{-1}(\Omega)\right|}\,, \tag{2.57b}$$

$$S_{xF}(\Omega) = -\frac{\hbar}{2}\,\frac{\operatorname{Re}\chi^{-1}(\Omega)}{\left|\operatorname{Im}\chi^{-1}(\Omega)\right|}\,, \tag{2.57c}$$

$$S_{\rm tot}(\Omega) = \hbar\left|\operatorname{Im}\chi^{-1}(\Omega)\right|\,. \tag{2.58}$$

The limit obtained in (2.58) is interesting because, just like the SQL, it depends only on the test object parameters and, moreover, exactly matches the expression for the thermal noise of the test object at zero temperature, even though the physical source of noises in (2.58) is another object, the meter. We also note that for a harmonic oscillator at the resonance frequency $\Omega = \Omega_{\rm m}$, Eqn (2.58) coincides with the SQL in (2.31), which is obviously connected with the fact that $\operatorname{Re}\chi^{-1} = 0$ for an oscillator at the resonance frequency.

Limit (2.58) is fundamentally unreachable because the thermal noise of the test object makes the same contribution even at zero temperature. To merely approach it, the temperature of the test object must be decreased to $T \lesssim \hbar\Omega/\kappa_{\rm B}$. For characteristic frequencies of the gravitational-wave signal (around 1 kHz or less), this corresponds to fractions of a microkelvin. Therefore, for a modern technological level, limit (2.58), unlike the SQL, can be considered a hypothetical one.

Based on Eqn (2.56), we can obtain another, more realistic and quite relevant sensitivity limit for laser gravita-

tional-wave detectors. In high-precision measurement systems, friction in the test object (that is, the quantity $\mathrm{Im}\,\chi^{-1}$) is minimized in order to decrease the thermal noise (see Section 2.4). Therefore, in all practical cases, the first term in (2.56) is many orders of magnitude higher than the second one, which allows disregarding the latter:

$$S_{\mathrm{tot}}(\Omega) = \frac{\hbar^2 \left|\chi^{-1}(\Omega)\right|^2}{4S_F(\Omega)} \,. \tag{2.59}$$

Formula (2.59) relates the quantum probe system sensitivity to the energy stored in it that is needed for the creation of the back-action on the test object. Hence, this limit was named the *energetic quantum limit* [63–66].

Notably, in laser interferometers, S_F is proportional to the optical power circulating in them, and due to limit (2.59) and the need for tremendous measurement precision, this power reaches very high values. In first-generation detectors, this power reached several dozen kilowatts [40], and in second-generation detectors, it should reach 1 MW [43]. As a result, a large number of undesired effects can appear in the interferometer, in particular, the distortion of mirror shapes due to their heating (thermal lensing) and the effect of optomechanical parametric instability predicted by Braginsky and coauthors [67, 68] in 2001 (recently, this effect was experimentally observed at LIGO [69]).

3. Quantum noises in laser interferometers

3.1 Michelson interferometer

3.1.1 Operation principle of laser gravitational-wave detectors. We consider the operation principle of laser gravitational-wave detectors using the simple example of the Michelson interferometer shown in Fig. 5.

The structure of the lines of the tidal acceleration field created by the gravitational wave is shown in Fig. 6. In such a field, with the optimal detector arm orientation, the following forces are applied to the test masses [3]:

$$F_{\mathrm{sign}\,1,2}(t) = \pm\frac{ML\ddot{h}(t)}{2} \,. \tag{3.1}$$

These forces are directed along the axes that connect the corresponding mass with the origin, which in this case is a beam splitter. Hence, in order to detect the action of the gravitational wave, we need to measure small variations of the test-mass coordinate difference

$$x = \frac{x_1 - x_2}{2} \,. \tag{3.2}$$

For this reason, laser radiation enters the interferometer through the 'bright' port (on the left-hand side of Fig. 5) and is evenly split by the beam splitter and is directed towards two test mirrors. After reflection, these waves acquire phase shifts proportional to the mirror coordinates. After recombination on the beam splitter in the case $x_1 = x_2$ (hypothetical), all light is reflected back to the laser. At the second port, known as the 'dark' port (lower part of Fig. 5), destructive interference occurs. If $x_1 \neq x_2$, then part of the light is directed into the dark port and is registered by the photodetector.

Here, we consider quantum fluctuations of light in such interferometers. We also show that they fully correspond to the general model of a linear probe system discussed in Section 2, and obtain explicit expressions for quantum noises $\hat{x}_{\mathrm{fl}}$ and $\hat{F}_{\mathrm{fl}}$.

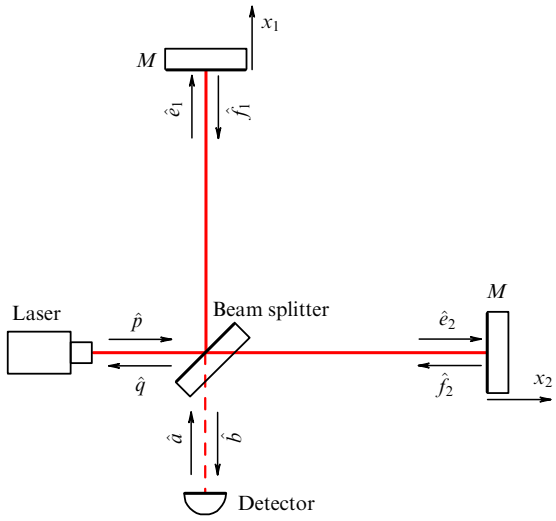

Figure 5. Simplified schematic of a laser gravitational-wave detector. M are the masses of movable mirrors.

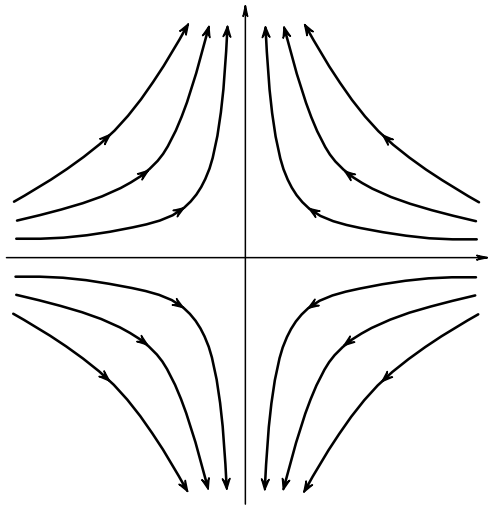

Figure 6. Structure of the tidal acceleration field lines of a gravitational wave propagating in the direction normal to the figure plane (figure orientation corresponds to the so-called + polarization; the structure corresponding to another polarization, known as the × polarization, can be obtained by simply rotating the figure through 45°).

To simplify the calculations, we first discuss the simplest Michelson interferometer in detail (see Fig. 5). Then, based on a qualitative approach, we generalize the obtained results to the case of a more complicated scheme of a power- and signal-recycled Fabry–Perot–Michelson interferometer (Fig. 7), which is actually used in modern gravitational-wave detectors.

3.1.2 Interferometer optical fields. The approach that is typically used for the analysis of quantum noises in laser gravitational-wave detectors, the so-called *two-photon formalism*,[3] was suggested in [70, 71]. Its simplified version, which is nevertheless appropriate for our calculations, is given in Appendix B.

[3] The etymology is connected with the term 'two-photon devices' used at that time in nonlinear optics.

According to this formalism, the laser radiation that enters the interferometer through the bright port is described by the expression

$$\hat{p}(t) = \left(P + \hat{p}^{\,\mathrm{c}}(t)\right)\cos(\omega_0 t) + \hat{p}^{\,\mathrm{s}}(t)\sin(\omega_0 t)\,, \tag{3.3}$$

where $\hat{p}^{\,\mathrm{c,s}}(t)$ are quadrature amplitude operators and the classical amplitude P is defined by the pump laser power I_0, which in this case coincides with the power I_{c} circulating inside the interferometer:

$$I_0 = I_{\mathrm{c}} = \frac{\hbar\omega_0 P^2}{2}\,. \tag{3.4}$$

An accurate analysis of quantum noises must take the radiation entering through the dark port into account:

$$\hat{a}(t) = \hat{a}^{\,\mathrm{c}}(t)\cos(\omega_0 t) + \hat{a}^{\,\mathrm{s}}(t)\sin(\omega_0 t)\,. \tag{3.5}$$

It can be produced just by zero fluctuations caused by the Planck radiation of the photodetector[4] or by specially prepared 'squeezed' light (this case is discussed in detail in Section 4.1).

The incoming fields combine on the central beam splitter, resulting in the following expressions for waves incident on the test masses M:

$$\hat{e}_{1,2}(t) = \frac{\hat{p}(t - L_{\mathrm{LM}}/c) \pm \hat{a}(t - L_{\mathrm{DM}}/c)}{\sqrt{2}}\,, \tag{3.6}$$

where L_{LM} is the optical distance between the laser and the mirrors and L_{DM} is the distance from the detectors to the mirrors. We assume that both these distances are proportional to an integer number of pump wavelengths; this assumption does not influence the generality of the considerations in any way, but simplifies the calculations. In addition, we also take into account that in real ground-based laser gravitational-wave detectors, the time intervals L_{LM}/c and L_{DM}/c are significantly smaller than the characteristic time of the gravitational-wave signal variation. Then expression (3.6) can be rewritten as

$$\hat{e}_{1,2}(t) = \hat{e}^{\,\mathrm{c}}_{1,2}(t)\cos(\omega_0 t) + \hat{e}^{\,\mathrm{s}}_{1,2}(t)\sin(\omega_0 t)\,, \tag{3.7}$$

where

$$\begin{pmatrix} \hat{e}^{\,\mathrm{c}}_{1,2}(t) \\ \hat{e}^{\,\mathrm{s}}_{1,2}(t) \end{pmatrix} = \frac{1}{\sqrt{2}}\left[\begin{pmatrix} P + \hat{p}^{\,\mathrm{c}}(t) \\ \hat{p}^{\,\mathrm{s}}(t) \end{pmatrix} \pm \begin{pmatrix} \hat{a}^{\,\mathrm{c}}(t) \\ \hat{a}^{\,\mathrm{s}}(t) \end{pmatrix}\right]. \tag{3.8}$$

For small values of the mirror displacements $\hat{x}_{1,2}$ from the initial positions, the waves reflected from them can be expressed as

$$\begin{aligned}\hat{f}_{1,2}(t) &= \hat{e}^{\,\mathrm{c}}_{1,2}(t)\cos\left\{\omega_0\left[t - \frac{2\hat{x}_{1,2}(t)}{c}\right]\right\} \\ &\quad + \hat{e}^{\,\mathrm{s}}_{1,2}(t)\sin\left\{\omega_0\left[t - \frac{2\hat{x}_{1,2}(t)}{c}\right]\right\} \\ &= \hat{f}^{\,\mathrm{c}}_{1,2}(t)\cos(\omega_0 t) + \hat{f}^{\,\mathrm{s}}_{1,2}(t)\sin(\omega_0 t)\,.\end{aligned} \tag{3.9}$$

[4] We recall that the energy of one optical quantum corresponds to the temperature of several dozen thousand kelvins and therefore room temperature is almost zero for light.

If second-order terms proportional to $\hat{p}^{\,\mathrm{c,s}}\hat{x}_{1,2}$ and $\hat{a}^{\,\mathrm{c,s}}\hat{x}_{1,2}$ are ignored, it is easy to show that

$$\begin{aligned}\begin{pmatrix} \hat{f}^{\,\mathrm{c}}_{1,2}(t) \\ \hat{f}^{\,\mathrm{s}}_{1,2}(t) \end{pmatrix} &= \frac{1}{\sqrt{2}}\left[\begin{pmatrix} P + \hat{p}^{\,\mathrm{c}}(t) \\ \hat{p}^{\,\mathrm{s}}(t) \end{pmatrix} \pm \begin{pmatrix} \hat{a}^{\,\mathrm{c}}(t) \\ \hat{a}^{\,\mathrm{s}}(t) \end{pmatrix}\right. \\ &\quad \left. + \frac{2\omega_0 P\hat{x}_{1,2}(t)}{c}\begin{pmatrix} 0 \\ 1 \end{pmatrix}\right].\end{aligned} \tag{3.10}$$

Finally, the waves formed after the recombination $\hat{f}_{1,2}$ at the beam splitter and directed back towards the laser and the black port have the following form (under the assumptions made above):

$$\hat{q}(t) = \frac{\hat{f}_1(t) + \hat{f}_2(t)}{\sqrt{2}} = \hat{q}^{\,\mathrm{c}}(t)\cos(\omega_0 t) + \hat{q}^{\,\mathrm{s}}(t)\sin(\omega_0 t)\,, \tag{3.11}$$

$$\hat{b}(t) = \frac{\hat{f}_1(t) - \hat{f}_2(t)}{\sqrt{2}} = \hat{b}^{\,\mathrm{c}}(t)\cos(\omega_0 t) + \hat{b}^{\,\mathrm{s}}(t)\sin(\omega_0 t)\,, \tag{3.12}$$

where

$$\begin{pmatrix} \hat{q}^{\,\mathrm{c}}(t) \\ \hat{q}^{\,\mathrm{s}}(t) \end{pmatrix} = \begin{pmatrix} P + \hat{p}^{\,\mathrm{c}}(t) \\ \hat{p}^{\,\mathrm{s}}(t) \end{pmatrix} + \frac{2\omega_0 P\hat{y}(t)}{c}\begin{pmatrix} 0 \\ 1 \end{pmatrix}, \tag{3.13}$$

$$\begin{pmatrix} \hat{b}^{\,\mathrm{c}}(t) \\ \hat{b}^{\,\mathrm{s}}(t) \end{pmatrix} = \begin{pmatrix} \hat{a}^{\,\mathrm{c}}(t) \\ \hat{a}^{\,\mathrm{s}}(t) \end{pmatrix} + \frac{2\omega_0 P\hat{x}(t)}{c}\begin{pmatrix} 0 \\ 1 \end{pmatrix}, \tag{3.14}$$

$$\hat{y}(t) = \frac{\hat{x}_1(t) + \hat{x}_2(t)}{2}\,. \tag{3.15}$$

It follows from Eqns (3.7)–(3.15) that after entering the interferometer, almost all the optical power is directed back to the bright port towards the laser; a small part of the input power that carries the information about $\hat{x}$ is directed to the dark port.

3.1.3 Measurement noise. In modern laser detectors, the radiation that escapes through the dark port is registered by a so-called homodyne detector, which allows measuring any linear combination of quadrature amplitudes $\hat{b}^{\,\mathrm{c}}$ and $\hat{b}^{\,\mathrm{s}}$. The output signal of a homodyne detector (see details, e.g., in [45]) is proportional to

$$i_-(t) \propto \hat{b}^{\,\mathrm{c}}\cos\zeta + \hat{b}^{\,\mathrm{s}}\sin\zeta\,, \tag{3.16}$$

where ζ is the so-called homodyne phase (we note that the detector output signal is already a classical observable, and therefore the exact form of the scaling factor in (3.16) is insignificant).

Substituting relations (3.14) in (3.16), we obtain

$$i_-(t) \propto \hat{a}^{\,\mathrm{c}}\cos\zeta + \left[\hat{a}^{\,\mathrm{s}}(t) + \frac{2\omega_0 P\hat{x}(t)}{c}\right]\sin\zeta\,. \tag{3.17}$$

Equation (3.17) can be written in a form similar to (2.1) by renormalizing it to the value of the input signal $\hat{x}$:

$$i_-(t) \propto \hat{x}(t) + \hat{x}_{\mathrm{fl}}(t)\,, \tag{3.18}$$

where

$$\hat{x}_{\mathrm{fl}}(t) = \frac{c}{2\omega_0 P}\left(\hat{a}^{\,\mathrm{c}}(t)\cot\zeta + \hat{a}^{\,\mathrm{s}}(t)\right) \tag{3.19}$$

is *shot noise*, which plays the role of the measurement quantum noise in laser interferometers.

3.1.4 Test-mass equations of motion. We now consider the evolution of the interferometer test mass coordinates $\hat{x}_{1,2}$. Besides forces (3.1) created by a gravitational wave, they are also influenced by the radiation pressure forces created by the optical field in the interferometer (because we are interested here only in quantum noises, thermal and other 'technological' noises F_T are ignored):

$$\hat{F}_{\mathrm{rad}\,1,2}(t) = \frac{2\hat{I}_{1,2}(t)}{c}\,, \tag{3.20}$$

where $\hat{I}_{1,2}$ are the values of the optical power circulating in each interferometer arm. Using Eqns (3.8), (B.8), and (B.9) (see Appendix B), it is easy to show that these forces include the same constant components I_c/c and fluctuating terms

$$\hat{F}_{\mathrm{fl}\,1,2}(t) = \frac{\hbar\omega_0 P}{c}\left(\hat{p}^{\,c}(t) \pm \hat{a}^{c}(t)\right). \tag{3.21}$$

Constant forces do not interest us here (in real gravitational-wave detectors, they result only in some offset of the suspended mirrors from the equilibrium position), and we do not consider them.

As a result, the equations of motion of the test mass take the form

$$M\,\frac{\mathrm{d}^2\hat{x}_1(t)}{\mathrm{d}t^2} = F_{\mathrm{sign}\,1}(t) + \hat{F}_{\mathrm{fl}\,1}(t)\,, \tag{3.22a}$$

$$M\,\frac{\mathrm{d}^2\hat{x}_2(t)}{\mathrm{d}t^2} = F_{\mathrm{sign}\,2}(t) + \hat{F}_{\mathrm{fl}\,2}(t)\,. \tag{3.22b}$$

Accordingly, for coordinate difference (3.2), we obtain the equations

$$m\,\frac{\mathrm{d}^2\hat{x}(t)}{\mathrm{d}t^2} = F_{\mathrm{sign}}(t) + \hat{F}_{\mathrm{fl}}(t) \tag{3.23}$$

[cf. the general equation (2.5)], where

$$m = 2M \tag{3.24}$$

is the reduced mass of interferometer mirrors,

$$F_{\mathrm{sign}}(t) = F_{\mathrm{sign}\,1}(t) - F_{\mathrm{sign}\,2}(t) = \frac{mL\ddot{h}(t)}{2} \tag{3.25}$$

is the differential signal force, and

$$\hat{F}_{\mathrm{fl}}(t) = \hat{F}_{\mathrm{fl}\,1}(t) - \hat{F}_{\mathrm{fl}\,2}(t) = \frac{2\hbar\omega_0 P\hat{a}^{c}(t)}{c} \tag{3.26}$$

is the *radiation pressure noise*, which plays the role of back-action noise in laser interferometers.

We note that fluctuations of both the amplitude and the phase of pump laser radiation influence neither the output signal nor the fluctuations of the light pressure force. Of course, this conclusion is valid only for an ideally symmetric interferometer, which we consider here. In real gravitational-wave detectors, there are very high requirements on the 'purity' of the pump laser radiation, which are realized, in particular, by using many feedback loops in the interferometer scheme [72]. However, without using the symmetric topology of the Michelson interferometer, any technical tricks would hardly provide such a quantum level of optical noises as in laser gravitational-wave detectors.

3.2 Power- and signal-recycling Fabry–Perot–Michelson interferometer

3.2.1 Fabry–Perot–Michelson interferometer. A key disadvantage of the considered scheme of a gravitational-wave detector based on the Michelson interferometer is the very low optomechanical interaction provided only by a single reflection from the movable mirror. Simple estimates show that in order to achieve the sensitivity needed for gravitational-wave detection in this case, an unrealistically high optical power of the order of several hundred megawatts is needed.

The Fabry–Perot–Michelson interferometer scheme practically used in modern detectors is shown in Fig. 7. In addition to the already considered Michelson interferometer end test-masses (ETMs), it can include up to four additional mirrors: two input test masses (ITMs) in the interferometer arms, a power-recycling mirror (PRM), and a signal-recycling mirror (SRM).

ITM mirrors that already appeared in early prototype interferometers are used in almost all laser gravitational-wave detectors [19]. Together with the end test masses, they transform the Michelson interferometer arms into Fabry–Perot cavities, where light circulates and acquires a proportionally increased phase shift. Due to multiple reflections of light from the mirrors, the influence of the back-action force on them increases by the same factor (in most early prototypes, instead of Fabry–Perot resonators, delay lines were used, having the same effect but being less workable for large arm lengths).

Calculations of quantum noises in Fabry–Perot–Michelson interferometers are given, e.g., in [45]. In this and other similar articles, the spectral representation is used as the more convenient one for analyzing stationary frequency selective devices; in what follows, we use this representation as well.

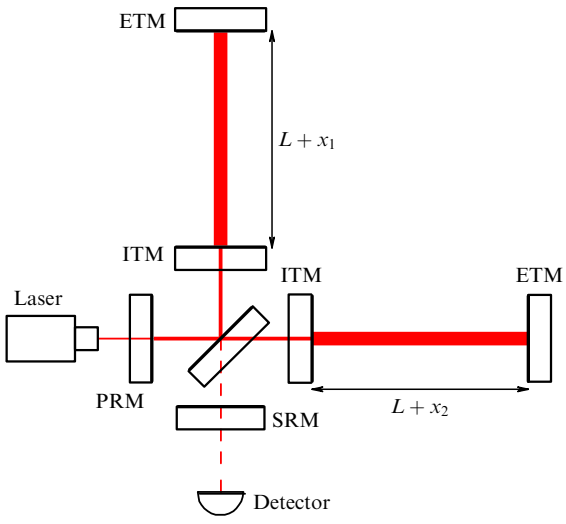

Figure 7. Schematic of a power- and signal-recycled Fabry–Perot–Michelson interferometer used in modern gravitational-wave detectors. ETM — end test masses, ITM — input test assess, PRM — power recycling mirror, SRM — signal recycling mirror.

The presence of Fabry–Perot cavities modifies Eqns (3.19) and (3.26) as follows:[5]

$$\hat{x}_{\text{fl}}(\Omega) = \frac{c}{2\omega_0 E\mathcal{L}^*(\Omega)}\left[\hat{a}^{\text{c}}(\Omega)\cot\zeta + \hat{a}^{\text{s}}(\Omega)\right], \tag{3.27}$$

$$\hat{F}_{\text{fl}}(\Omega) = \frac{2\hbar\omega_0 E\mathcal{L}(\Omega)}{c}\,\hat{a}^{\text{c}}(\Omega). \tag{3.28}$$

Here,

$$\mathcal{L}(\Omega) = \frac{\sqrt{c\gamma/L}}{\gamma - \text{i}\Omega} \tag{3.29}$$

is a dimensionless factor that describes the resonance light amplification in Fabry–Perot cavities,

$$\gamma = \frac{c}{L}\,\frac{1-\sqrt{R_{\text{ITM}}}}{1+\sqrt{R_{\text{ITM}}}} \approx \frac{cT_{\text{ITM}}}{4L} \tag{3.30}$$

is the FWHM of the Fabry–Perot transmission band, R_{ITM} and T_{ITM} are reflection and transmission coefficients of ITM mirrors, and E is the effective classical amplitude of light in the cavity, defined by the relation

$$I_{\text{c}} = \frac{\hbar\omega_0 E^2}{2} = I_0\left|\mathcal{L}(0)\right|^2, \tag{3.31}$$

where I_{c} is the total optical power circulating in two interferometer arms.

The presence of two additional mirrors also modifies mechanical equations of motion (3.22a), (3.22b), and (3.23) (see [45]). In the first two equations, the mass M is replaced by the reduced mass of the mirrors ITM + ETM, i.e., if they have the same masses, M is replaced by $M/2$. Correspondingly, the reduced mass for the whole interferometer in Eqn (2.23) is

$$m = 2\times\frac{M}{2} = M. \tag{3.32}$$

3.2.2 Power recycling. It follows from Eqn (3.31) that the smaller γ is, the larger the circulating power I_{c} for a fixed pump laser power I_0. On the other hand, as can be seen from Eqn (3.27), the lifetime of light in Fabry–Perot cavities $1/\gamma$ cannot be increased arbitrarily, because the cavities smooth the spectral components of a gravitational signal with frequencies Ω higher than γ, which leads to an increase (normalized to the input) in the measurement noise at these frequencies. High-frequency spectral components of light power fluctuations are smoothed as well, which leads to a decrease in the back-action noise for $\Omega > \gamma$ [see Eqn (3.28)].

The idea of using a power-recycling mirror was introduced by Drever as a solution to the mentioned contradiction [73]. According to its name, this mirror returns the larger part of the power that escapes through the bright port back into the interferometer. In other words, this mirror, together with two input test masses, forms an effective composite mirror with a very low transmission coefficient:

$$\frac{T_{\text{PRM}}T_{\text{ITM}}}{\left(1+\sqrt{R_{\text{PRM}}R_{\text{ITM}}}\,\right)^2} \approx \frac{T_{\text{PRM}}T_{\text{ITM}}}{4}, \tag{3.33}$$

where R_{PRM} and T_{PRM} are the reflection and transmission coefficients of the PRM. This leads to a manifold increase in the power circulating in the interferometer. This does not influence the transmission band for the signal light, because it is not transmitted through the bright port.

We also note that this composite mirror and the end mirrors form a very narrow-band effective Fabry–Perot cavity for pump radiation (with a bandwidth of several Hertz). In laser gravitational-wave detectors, the pump laser frequency is related via the feedback loop to the frequency of this cavity, providing a record-high stability of the pump laser.

A configuration with Fabry–Perot cavities in the arms and an additional power-recycling mirror was used in most first-generation laser gravitational-wave detectors, including TAMA 300, Virgo, and LIGO.

3.2.3 Signal recycling. Similarly to the power-recycling mirror, the signal-recycling mirror and the ITM form an effective composite mirror, which, in turn, together with the ETM mirrors, forms an effective Fabry–Perot cavity, but in this case for the radiation passing through the dark port. This idea was first introduced by Meers [74] as a tool for easy optimization of the transfer function spectral form in laser gravitational-wave detectors for different types of gravitational-wave signals. Indeed, depending on the optical distance between the recycling mirror and the ITM mirrors, the transmission coefficient of a composite mirror can be varied from the minimal value, similar to (3.33), to the maximal value

$$\frac{T_{\text{SRM}}T_{\text{ITM}}}{\left(1-\sqrt{R_{\text{SRM}}R_{\text{ITM}}}\,\right)^2} \approx \frac{4T_{\text{SRM}}T_{\text{ITM}}}{\left(T_{\text{SRM}}+T_{\text{ITM}}\right)^2}. \tag{3.34}$$

In the intermediate cases, the reflected wave also experiences some phase shift, which makes the behavior of this system even more complicated (the same is in principle valid for the PRM, but this mirror, obviously, is always adjusted in such a way that the transmission is minimal).

The signal-recycling mirror is used in ALIGO detectors and, presumably, will be used in other second-generation detectors, but most probably only for one type of adjustment, which provides maximal transmission of an ITM + SRM composite mirror and, accordingly, the maximal width of the interferometer transmission band. The choice of this regime is justified by the combination of two technological reasons connected with features inherent in second-generation detectors.

On the one hand, optimization of quantum noise in second-generation detectors requires a maximally 'flat' shape of its spectral density, which is realized for a wide interferometer transmission band, $\gamma \gtrsim 2\pi\times 500$ Hz [75], and hence (if the SRM is not used) for very large values $T_{\text{ITM}} \gtrsim 0.15$ [see Eqn (3.30)]. This is because the spectral density of Brownian fluctuations of reflective dielectric coating widths of the mirrors, being the main technological noise in these detectors, has a quite weak dependence on the frequency (see Fig. 2 in [43]), which dictates a similar 'flat' shape of the quantum noise spectral density.

On the other hand, the planned optical power values in the arms of second-generation detectors are near several hundred kilowatts, which for such large values of T_{ITM} corresponds to several tens of kilowatts transmitted through the input mirrors and the beam splitter. Problems with heat release and various undesirable nonlinear effects, which are inevita-

[5] Equations (3.27) and (3.28) are obtained using the so-called single-mode approximation: $\Omega \ll c/L$ and $\gamma \ll c/L$; for the limit transition to the case without Fabry–Perot cavities, we should set $\Omega \ll \gamma = c/L$.

ble at such powers, make such a system nonapplicable. Thus, in ALIGO interferometers, input mirrors are used with a transmission one order of magnitude smaller ($T_{\rm ITM} = 0.014$), which corresponds to a moderate power of approximately 5 kW on the beam splitter (for the power $\approx$ 800 kW planned in the arms). This leads to a very narrow transmission band of Fabry–Perot cavities:

$$\gamma_{\rm arm} = \frac{cT_{\rm ITM}}{4L} = 2\pi \times 40 \text{ Hz}\,. \tag{3.35}$$

Using the signal-recycling mirror (or, more precisely, following the terminology in [76], the signal-extraction mirror) with the transmission coefficient $T_{\rm SRM} \approx 0.2-0.3$ allows resolving this contradiction. According to Eqn (3.34), the interferometer transmission band in this case broadens by more than one order of magnitude.

In conclusion, we note for completeness that a configuration without input mirrors in the arms is possible, with the power- and signal-recycling mirrors providing all the required interferometer parameter values. This setup is used in the GEO 600 gravitational-wave detector [38]. One disadvantage of this setup is that all power circulating in the interferometer arms passes through the beam splitter. This is applicable for relatively small first-generation GEO 600 detector, in which this power is only several kilowatts, but not for second-generation detectors.

3.3 Spectral density of quantum noises

Using relations (3.27) and (3.28) and taking into account that γ is the FWHM of the interferometer as a whole and depends on both $T_{\rm ITM}$ and $T_{\rm SRC}$, it is easy to obtain explicit expressions for quantum noise spectral densities in laser interferometers. In the simplest particular case where only vacuum fluctuations enter the dark port (i.e., the light squeezing technology considered in Section 4.1 is not used) [see Eqn (B.14)], they have the form

$$S_x(\Omega) = \frac{\hbar}{2m\Omega^2\mathcal{K}(\Omega)\sin^2\zeta}\,, \tag{3.36a}$$

$$S_F(\Omega) = \frac{\hbar m\Omega^2\mathcal{K}(\Omega)}{2}\,, \tag{3.36b}$$

$$S_{xF}(\Omega) = \frac{\hbar}{2}\cot\zeta\,, \tag{3.36c}$$

where

$$\mathcal{K}(\Omega) = \frac{2\Theta\gamma}{m\Omega^2(\gamma^2+\Omega^2)} \tag{3.37}$$

is a convenient dimensionless factor introduced in [77] to describe the strength of optomechanical coupling in interferometers (Kimble's factor), and

$$\Theta = \frac{4\omega_0 I_{\rm c}}{cL} \tag{3.38}$$

is the normalized optical power circulating in the interferometer. It is easy to show using simple calculations that these spectral densities satisfy uncertainty relation (2.4), realizing the exact equality.

In first-generation laser detectors, where the circulating optical power was relatively small and did not exceed several tens of kilowatts, the value of $\mathcal{K}(\Omega)$ was small in the entire operating frequency range. Therefore, the radiation pressure noise influence on sensitivity was not noticeable in these detectors and the notion of 'quantum noise suppression' was equivalent to that of 'shot noise suppression'.

In this situation, an obvious strategy is to measure the phase quadrature of the light escaping through the dark port (because precisely this quadrature carries the information on the gravitational signal [see Eqn (3.14)]), which corresponds to the choice of the homodyne phase $\zeta = \pi/2$. As a result of this classical optimization, the measurement and back-action noises become uncorrelated and the detector sensitivity becomes limited by the SQL.

In first-generation detectors, this factor did not play any significant role, but in second-generation detectors, after they reach the planned sensitivity, the radiation pressure noise and hence the SQL will become noticeable factors that limit the sensitivity. However, in the nearest future, these detectors will still be operating in the classical optimization regime.

Equations (3.36) are in this case simplified as follows:

$$S_x(\Omega) = \frac{\hbar}{2m\Omega^2\mathcal{K}(\Omega)}\,, \tag{3.39a}$$

$$S_F(\Omega) = \frac{\hbar m\Omega^2\mathcal{K}(\Omega)}{2}\,, \tag{3.39b}$$

$$S_{xF}(\Omega) = 0\,. \tag{3.39c}$$

Substituting these spectral densities in expression (2.21) and taking into account that the test mirrors in laser gravitational-wave detectors can be regarded as free masses, it is easy to obtain the following expression for the total quantum noise spectral density in the h-normalization:

$$S^h_{\rm tot}(\Omega) = \frac{S^h_{\rm SQL}(\Omega)}{2}\left(\frac{1}{\mathcal{K}(\Omega)} + \mathcal{K}(\Omega)\right). \tag{3.40}$$

Expression (3.40) is different from the expression obtained in (2.27) for an abstract linear probe system by a more complicated dependence on the frequency, which appears due to the finiteness of the interferometer transmission band. For the frequencies within this band, Eqns (2.27) and (3.40) coincide up to the substitution

$$\Omega_{\rm q}^2 = \frac{2\Theta}{m\gamma}\,. \tag{3.41}$$

Spectral density (3.40) for the ALIGO parameters[6]

$$L = 4 \text{ km}\,, \tag{3.42a}$$

$$m = 40 \text{ kg}\,, \tag{3.42b}$$

$$\omega_0 = \frac{2\pi c}{1064 \text{ nm}} = 1.77\times10^{15} \text{ s}^{-1}\,, \tag{3.42c}$$

$$\frac{\Theta}{m} = (2\pi\times100)^3 \text{ s}^{-3} \Rightarrow I_{\rm c} = 2\times840 \text{ kW} \tag{3.42d}$$

and several typical values of γ is shown in Fig. 8.

[6] We specify the planned value of the optical power. During the first run of scientific observations, it was $\approx 2\times100$ kW.

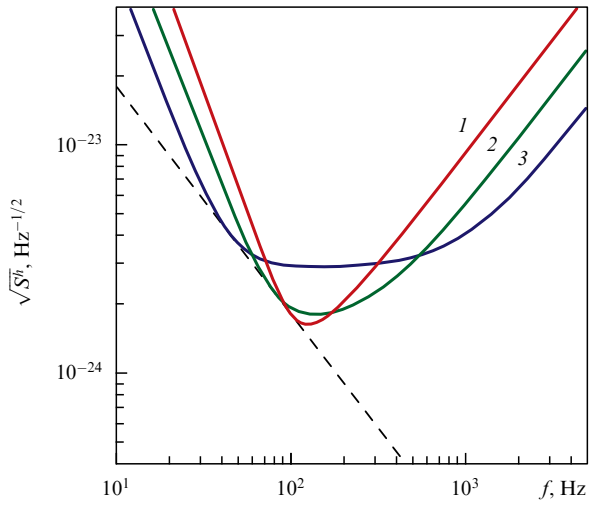

Figure 8. The total quantum noise spectral densities for the ALIGO parameters (3.42) and $\gamma = 2\pi \times 100\ \mathrm{s}^{-1}$ (curve *1*), $\gamma = 2\pi \times 300\ \mathrm{s}^{-1}$ (curve *2*), and $\gamma = 2\pi \times 1000\ \mathrm{s}^{-1}$ (curve *3*). Dashed line shows the SQL.

4. Methods for quantum noise suppression in laser interferometers

4.1 Squeezed light

4.1.1 Idea of using squeezed light in interferometers. An obvious method for decreasing the measurement noise of spectral density (3.39a) is to increase the parameter Θ, that is, the optical power I_c circulating in the interferometer arms. However, as mentioned in Section 2.5, there are finite limits for the application of this 'brute force' method.

An alternative approach was suggested by Caves [41]. The idea was to decrease the phase quadrature quantum uncertainty for the radiation that enters the interferometer through the dark port, which (for $\zeta = \pi/2$) gives a proportional decrease in the shot noise [see Eqns (3.19) and (3.27)]. Due to the commutation relation [see Eqn (B.2b) in Appendix B], this leads to a proportional increase in the second (amplitude) quadrature uncertainty $\hat{a}^c$ and, correspondingly, an increase in radiation pressure noise (3.28), such that uncertainty relation (2.18) remains valid.

4.1.2 Technology of light squeezing in interferometers. The preparation method for such *squeezed* quantum states is based on the process of degenerate parametric amplification: in an oscillator with a characteristic resistance modulated at its doubled eigenfrequency, one of the quadrature amplitudes is amplified, while the other is suppressed [78]. This process is illustrated in Fig. 9, where regions of quadrature amplitude uncertainties (that is, the cross section of the Wigner function at $1/\sqrt{\mathrm{e}}$ of the maximal value [79]) are shown for a zero (initial) state, some arbitrary squeezed state, and a squeezed state with reduced uncertainty of the quadrature $\hat{a}^s$.

The first experiments on squeezed light generation were performed in the mid-1980s [80]. However, the technology of preparing squeezed light states in which the spectral density of fluctuations of one of the quadratures would be reduced to a level lower than the zero-point fluctuation level at the operating frequencies of gravitational-wave detectors [which are very low compared with 'conventional' quantum optics

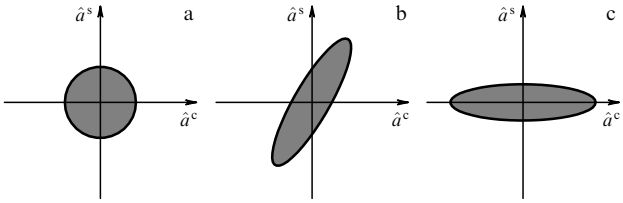

Рис. 9. Uncertainty regions for the quadrature amplitudes: (a) the initial state; (b) a squeezed state with an arbitrary θ; and (c) a squeezed state with $\theta = 0$.

(down to several Hertz)] was developed only in the 21st century [81–83].

The first practical application of squeezed light in gravitational-wave detectors happened in 2011, when the squeezing scheme was added to the GEO 600 detector [84, 85]. The injection of squeezed light allowed decreasing shot noise and hence increasing the sensitivity of this detector at high frequencies by approximately 3 dB (at the same optical power). Since that time, the GEO 600 detector has continued to routinely operate in the squeezing regime.

At the end of 2011, at the very end of the life cycle of the Initial LIGO detectors, the application of squeezed light was also tested in one of them [42]. Squeezed light is not yet used in the ALIGO detectors, but there is no doubt that this is a temporary situation.

A simplified scheme of squeezed light generation and injection into the interferometer is shown in Fig. 10 (see also Fig. 1 in [84], where it is shown in greater detail). Light with a frequency ω_0 either comes from the main pump laser or is generated by a separate laser synchronized with it (we note that this laser determines the squeezing phase θ, which should be very accurately linked to the pump laser phase) and is then sent into the second harmonic generator. Output radiation of that generator with the frequency $2\omega_0$ pumps the degenerate optical parametric oscillator, which uses the principle described above and generates a 'squeezed vacuum' (Fig. 9c), again at the frequency ω_0.

Further, this light is sent into the interferometer dark port instead of zero-point fluctuations coming from the photodetector. This is achieved by using an optical circulator consisting of a polarization beam splitter and a Faraday polarization rotator. The circulator directs the squeezed light into the

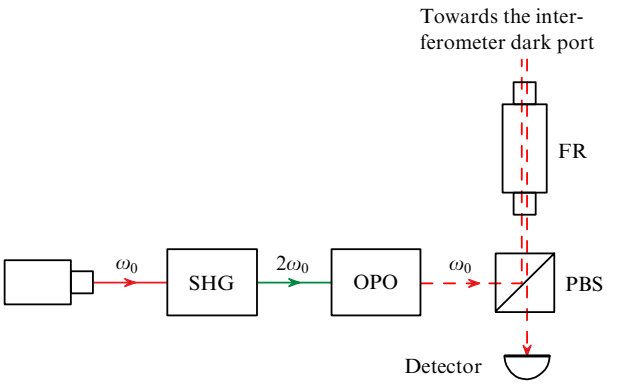

Figure 10. Schematic for squeezed light generation and injection into the interferometer. SHG — second harmonic generator, OPO — optical parametric oscillator, PBS — polarization beam splitter, FR — Faraday rotator. The last two elements form an optical circulator that separates the interferometer input and output beams.

interferometer and sends the interferometer output signal to the detector, while the photodetector zero-point fluctuations (not shown in Fig. 10) are reflected from the polarization beam splitter and do not enter the interferometer.

4.1.3 Quantum noise spectral densities. In the case where squeezed light is used, the relations for quantum noise spectral densities can be obtained by combining Eqns (3.27), (3.28), and (B.17):

$$S_x(\Omega) = \frac{\hbar}{2m\Omega^2\mathcal{K}(\Omega)} \frac{\cosh(2r) + \sinh(2r)\cos\left[2(\theta-\zeta)\right]}{\sin^2\zeta}, \tag{4.1a}$$

$$S_F(\Omega) = \frac{\hbar m\Omega^2\mathcal{K}(\Omega)}{2}\left[\cosh(2r) + \sinh(2r)\cos(2\theta)\right], \tag{4.1b}$$

$$S_{xF}(\Omega) = \frac{\hbar}{2}\frac{\cosh(2r)\cos\zeta + \sinh(2r)\cos(2\theta-\zeta)}{\sin\zeta}. \tag{4.1c}$$

We concentrate on the case where there is no cross-correlation between the shot noise and radiation pressure noise. As we have mentioned, this case applies to first- and second-generation gravitational-wave detectors and is realized for $\zeta = \pi/2$ and $\theta = 0$. Equations (4.1) and the total quantum noise relation take the form

$$S_x(\Omega) = \frac{\hbar}{2m\Omega^2\mathcal{K}(\Omega)}\exp(-2r), \tag{4.2a}$$

$$S_F(\Omega) = \frac{\hbar m\Omega^2\mathcal{K}(\Omega)}{2}\exp(2r), \tag{4.2b}$$

$$S_{xF}(\Omega) = 0, \tag{4.2c}$$

$$S^h_{\rm tot}(\Omega) = \frac{S^h_{\rm SQL}(\Omega)}{2}\left[\frac{\exp(-2r)}{\mathcal{K}(\Omega)} + \mathcal{K}(\Omega)\exp(2r)\right]. \tag{4.3}$$

It is easy to see that Eqns (4.2) and (4.3) differ from the corresponding equations in the case of no squeezing, (3.39) and (3.40), only by the factor $\exp(2r)$. This means that the squeezed light injection has the same effect on the quantum noise as the proportional change in the optical power.

Figure 11 shows the total quantum noise spectral densities without squeezing and with a 10 dB squeezing for ALIGO parameters (3.42) and $\gamma = 2\pi\times 300\ \mathrm{s}^{-1}$. These plots clearly demonstrate the sensitivity improvement at high and intermediate frequencies, where shot noise is dominant, and the sensitivity degradation at low frequencies, where radiation pressure noise dominates.

There are a number of methods that provide the sensitivity improvement for all frequencies, and they are discussed in Section 4.2. All these methods require more significant changes to the interferometer topology than just simply adding the squeezing. But there is a simple technique that does not require such topology changes and allows increasing the sensitivity at high and intermediate frequencies without decreasing the low-frequency sensitivity.

4.1.4 Quantum noise optimization using squeezed light. We discuss the structure of expression (4.3) in more detail. We can see that if

$$\Omega_{\rm q} = \sqrt{\frac{2\Theta\exp(2r)}{m\gamma}} < \gamma \tag{4.4}$$

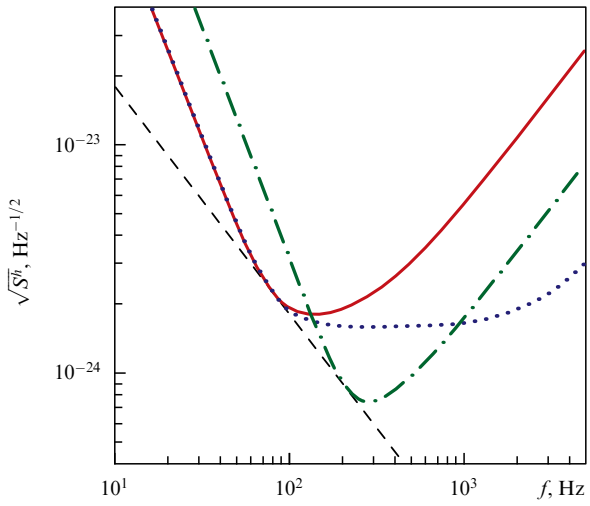

Figure 11. Squeezing influence on the total quantum noise spectral density. Solid curve: $\gamma = 2\pi\times 300\ \mathrm{s}^{-1}$, no squeezing. Dashed-dotted line: $\gamma = 2\pi\times 300\ \mathrm{s}^{-1}$ and $\exp(2r) = 10$. Dotted line: $\gamma = 2\pi\times 3000\ \mathrm{s}^{-1}$ and $\exp(2r) = 10$. Dashed line: the SQL. All parameters that are not specified explicitly correspond to ALIGO [see (3.42)].

(which holds in all real laser gravitational-wave detectors), then Eqn (4.3) can be approximated as follows:

$$S^h_{\rm tot}(\Omega) \approx \frac{4\hbar}{mL^2}\begin{cases} \dfrac{2\Theta\exp(2r)}{m\Omega^4\gamma} \propto \dfrac{\exp(2r)}{\gamma}, & \Omega < \Omega_{\rm q}, \\ \dfrac{m\gamma\exp(-2r)}{2\Theta} \propto \gamma\exp(-2r), & \Omega_{\rm q} < \Omega < \gamma, \\ \dfrac{m\Omega^2\exp(-2r)}{2\Theta\gamma} \propto \dfrac{\exp(-2r)}{\gamma}, & \Omega > \gamma. \end{cases} \tag{4.5}$$

Hence, if we simultaneously introduce squeezing and broaden the interferometer transmission band proportionally to the squeezing factor $\exp(2r)$, then, compared with the initial conditions with no squeezing, the quantum noise does not change for low and middle frequencies, but at high frequencies the spectral density of this noise decreases by the factor $\exp(4r)$ (see the corresponding curve in Fig. 11). Compared with the case with squeezing but with the unchanged transmission band, the quantum noise spectral density decreases by the factor $\exp(2r)$ at low and high frequencies, but proportionally increases at intermediate frequencies. However, due to the above-mentioned character of technological noises in second-generation gravitational-wave detectors, there is no need for a significant reduction in quantum noise in the intermediate frequency range.

To summarize, the above discussion shows that in order to achieve sensitivity improvement (at least in second-generation detectors), it is necessary to simultaneously introduce squeezing and proportionally broaden the interferometer transmission band.

4.1.5 Influence of optical losses. The actual sensitivity improvement at high frequencies demonstrated by the GEO 600 and LIGO detectors [42, 84] was approximately 3 dB, while the squeezing factor at the interferometer input was approximately 10 dB in both cases. The reason for this difference is optical losses in the interferometers, which significantly lower the effective squeezing factor.

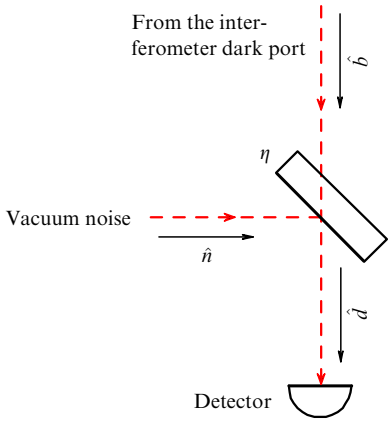

Figure 12. Model for optical losses in the interferometer output channel: $\eta < 1$ is the unified quantum efficiency, $\hat{n}$ is additional vacuum noise introduced by the optical losses.

In first- and second-generation detectors, the main contribution to these losses was made by the elements of the interferometer optical output channel (including the non-unit quantum efficiency of the photodetector). To calculate the influence of these losses, it is convenient to use the equivalent optical setup shown in Fig. 12. Here, the losses are modeled by a semi-transparent mirror, which transmits only a fraction $\eta < 1$ of the light escaping from the dark port to the detector (which in this case is ideal). The factor η, which characterizes all optical losses in the output channel, is known as the 'unified quantum efficiency' of the interferometer. The same mirror also adds effective vacuum noise $\hat{n}$ to the output signal (we recall that according to the fluctuation–dissipation theorem, any losses are accompanied by the introduction of the corresponding noise).

As a result, the following relation is valid for light incident on the photodetector:

$$\hat{d} = \sqrt{\eta}\,\hat{b} + \sqrt{1-\eta}\,\hat{n} = \sqrt{\eta}(\hat{b} + \epsilon\hat{n})\,, \tag{4.6}$$

where ϵ are the normalized optical losses,

$$\epsilon^2 = \frac{1-\eta}{\eta}\,. \tag{4.7}$$

This means that the shot noise spectral density in an interferometer with losses can be obtained using the rule

$$S_x = S_x^{\text{without loss}} + \epsilon^2 S_x^{\text{without loss and squeezing}}\,, \tag{4.8}$$

where the second term is created by the additional noise $\hat{n}$. In particular, in the case without squeezing, Eqn (3.39a) is modified to

$$S_x(\Omega) = \frac{\hbar}{2m\Omega^2\mathcal{K}(\Omega)\eta}\,, \tag{4.9}$$

and the addition of squeezing (4.2a) results in the expression

$$S_x(\Omega) = \frac{\hbar}{2m\Omega^2\mathcal{K}(\Omega)}\left[\exp(-2r) + \epsilon^2\right]. \tag{4.10}$$

We can conclude that if the unified quantum efficiency is *relatively* close to unity, $\eta \gtrsim 0.5$, as in modern laser gravitational-wave detectors, then in the case without squeezing the sensitivity decrease caused by the optical losses is relatively small. At the same time, these losses easily compensate the possible squeezing-assisted sensitivity improvement.

We consider the estimates for the GEO 600 detector presented in [84] as an example: the initial squeezing 10 dB ($\exp(-2r) \approx 0.1$) and the unified quantum efficiency $\eta \approx 0.62$. The effective squeezing is then given by

$$\exp(-2r) + \epsilon^2 \approx 0.71\,, \tag{4.11}$$

which is approximately only 1.5 dB. The sensitivity improvement compared with the case without squeezing and with the same losses is

$$\eta\exp(-2r) + 1 - \eta \approx 0.44\,, \tag{4.12}$$

which corresponds to the same 3.5 dB reported in [84].

4.2 Frequency-dependent squeezing and variation measurement

4.2.1 Frequency-dependent squeezing. A natural development of the idea to use squeezed light states is the introduction of frequency dependence into the squeezing phase θ, suggested by Unruh in [59]. Unruh showed that for any fixed observation frequency Ω, there is some optimal squeezing phase that provides the minimal total quantum noise at this frequency (the case $\theta = 0$ considered in Section 4.1 corresponds to the optimal squeezing phase value for $\Omega \to \infty$). Therefore, the optimal frequency dependence of θ can result in quantum noise suppression at all frequencies.

The expression for the total quantum noise spectral density in the case of an arbitrary phase squeezing can be obtained by substituting Eqns (4.1) in (2.15). To simplify the calculations, we once again limit our consideration to the special case $\zeta = \pi/2$. Then

$$S_{\text{tot}}^h(\Omega) = \frac{S_{\text{SQL}}^h(\Omega)}{2}\left\{\frac{\cosh(2r) - \sinh(2r)\cos(2\theta)}{\mathcal{K}(\Omega)}\right.$$
$$\left. - 2\sinh(2r)\sin(2\theta) + \mathcal{K}(\Omega)\left[\cosh(2r) + \sinh(2r)\cos(2\theta)\right]\right\}. \tag{4.13}$$

It is easy to show that for any fixed frequency Ω, if

$$\tan\theta(\Omega) = \mathcal{K}(\Omega)\,, \tag{4.14}$$

then the spectral density reaches its minimum:

$$S_{\text{tot}}^h(\Omega) = \frac{S_{\text{SQL}}^h(\Omega)}{2}\left(\frac{1}{\mathcal{K}(\Omega)} + \mathcal{K}(\Omega)\right)\exp(-2r)\,. \tag{4.15}$$

Comparing (4.15) and (3.40) shows that if squeezed light with the squeezing phase optimized in accordance with (4.14) is sent to the interferometer input, the quantum noise spectral density can be decreased by a factor of $\exp(2r)$ at all frequencies. Notably, this leads to the quantum noise spectral density being lower than the SQL in a broad frequency band, which is caused by a nonzero cross-correlation of the shot noise and the radiation pressure noise for $\theta \neq 0$ and $\theta \neq \pi/2$ [see the second term in braces in (4.13)].

Figure 13 shows spectral density (4.13) for several fixed values θ and optimized spectral density (4.15).

4.2.2 Variation measurement. A more radical approach, which in principle allows fully eliminating the influence of radiation

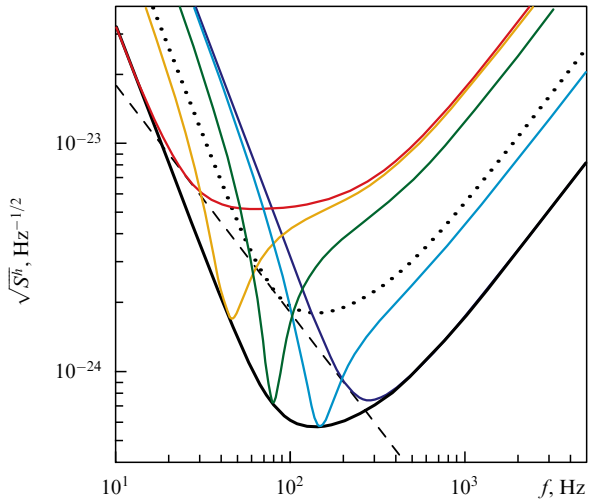

Figure 13. Influence of the squeezing phase θ on the total quantum noise spectral densities. Dotted curve: no squeezing. Thin solid curves: $\exp(2r) = 10$, θ is varied (in ascending order for positions of the minima) from $\pi/2$ to 0. Bold solid curve: $\exp(2r) = 10$ and optimized frequency-dependent squeezing phase (4.14). In all cases, $\gamma = 2\pi \times 300$ s^{-1}. Dashed line: SQL. All parameters not specified explicitly correspond to ALIGO [see (3.42)].

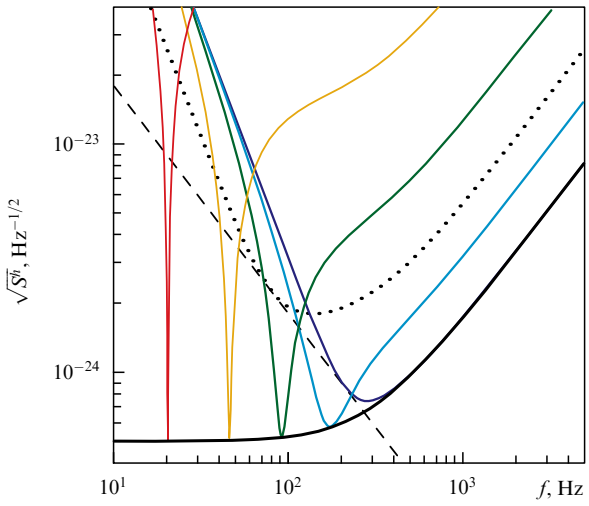

Figure 14. Homodyne phase ζ influence on the total quantum noise spectral densities. Dotted curve: no squeezing, $\zeta = \pi/2$. Thin solid curves: $\exp(2r) = 10$, $\theta = 0$, ζ is varied (in ascending order for positions of the minima) from 0.02π to $\pi/2$. Bold solid curve: $\exp(2r) = 10$, $\theta = 0$, and optimal frequency-dependent homodyne phase (4.17). In all cases, $\gamma = 2\pi \times 300$ s^{-1}. Dashed line: SQL. All parameters not specified explicitly correspond to ALIGO [see (3.42)].

pressure noise on the output signal of the interferometer, is the optimization of the cross-correlation spectral density S_{xF} considered in Section 2.5 [see Eqn (2.55)]. This optimization can be achieved in laser interferometers by introducing an (efficient) frequency dependence into the homodyne phase ζ [86, 87]. This approach is known as the variation measurement [77, 88].

It follows from (2.59) that the total quantum noise spectral density after such optimization is inversely proportional to S_F. Consequently, when using squeezed light, it is beneficial to choose the squeezing phase such that it provides the maximal value of S_F, which corresponds to $\theta = 0$. Combining Eqns (2.15) and (4.1) in this case, we obtain

$$S^h_{\rm tot}(\Omega) = \frac{S^h_{\rm SQL}(\Omega)}{2}\left[\frac{\exp(-2r) + \exp(2r)\cot^2\zeta}{\mathcal{K}(\Omega)} - 2\exp(2r)\cot\zeta + \mathcal{K}(\Omega)\exp(2r)\right]. \tag{4.16}$$

Spectral density (4.16) reaches its maximum for any fixed frequency Ω when

$$\cot\zeta(\Omega) = \mathcal{K}(\Omega) \tag{4.17}$$

[the same result can be obtained using the general expression (2.55)]. The corresponding optimized spectral density of the total quantum noise has the form

$$S^h_{\rm tot}(\Omega) = \frac{S^h_{\rm SQL}(\Omega)}{2}\frac{\exp(-2r)}{\mathcal{K}(\Omega)}. \tag{4.18}$$

It is easy to see that expression (4.18) corresponds to shot noise (4.2a) up to the recalculation between the coordinate spectral density and S^h. This means that the radiation pressure noise can indeed be fully suppressed by using the frequency-dependent homodyne phase.

Figure 14 shows spectral density (4.16) for several values of ζ and optimized spectral density (4.18).

4.2.3 Filter cavity. An obvious problem that arises when realizing frequency dependences (4.14) and (4.17) is that the characteristic frequencies $\Omega/(2\pi)$ in gravitational-wave detectors lie in the range from several Hertz to several kilohertz, and are therefore negligibly small in comparison with the optical frequencies, which requires certain devices with a very strong dispersion. It was suggested in [77] to use high-quality Fabry–Perot optical cavities as such devices.

It was also shown in [77] that after the reflection of squeezed light from such a *filter* cavity (Fig. 15), the squeezing phase is shifted by

$$\theta_{\rm f}(\Omega) = \arctan\frac{2\gamma_{\rm f}\delta_{\rm f}}{\gamma_{\rm f}^2 - \delta_{\rm f}^2 + \Omega^2}, \tag{4.19}$$

where $\gamma_{\rm f}$ and $\delta_{\rm f}$ are respectively the FWHM of the filter cavity transmission band and its detuning from the frequency ω_0. To realize the fourth-order dependence on Ω, which follows from (3.37) and (4.14), it was suggested to use two cavities connected in series. 'Conventional' squeezed light (with a frequency-independent phase θ) is sent to the input of the first cavity and the output of the second cavity is directed into the interferometer dark port. The authors of [77] named the setup with such a topology *pre-filtering*.

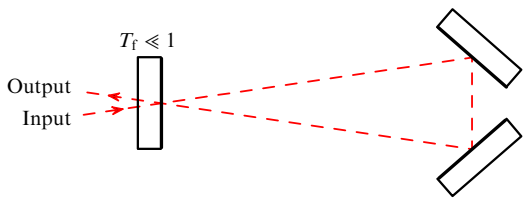

Figure 15. Filter cavity schematic [77]. Mirror on the left has a small transmission coefficient $T_{\rm f}$, while the other two are totally reflective. The triangular cavity is shown for clarity, because in this case the output beam is topologically separated from the input beam. It is possible to also use a linear cavity, but with an optical circulator similar to the one shown in Fig. 10.

It was shown in the same paper that such a cavity combination can also be used to achieve an effective frequency-dependent homodyne phase (4.17). For this purpose, the light escaping from the interferometer dark port should be sent to its input and the output signal should be registered with a homodyne detector. The authors called this the *post-filtering* setup.

Strictly speaking, the filter cavities in such a setup do not change the homodyne phase, but instead compensate the frequency dependence of the ponderomotive light squeezing introduced by the frequency-dependent optomechanical interaction in the interferometer [86]. This allows making optimal measurements of the output light with a 'conventional' homodyne detector (with a frequency-independent homodyne phase). However, the result fully corresponds to the one with a frequency-dependent homodyne phase.

4.2.4 Influence of optical losses in the interferometer. Comparing the obtained results, we conclude that the post-filtering scheme, which allows fully eliminating the radiation pressure noise, is better than the pre-filtering scheme, which can decrease it 'only' by a factor of $\exp(2r)$. However, this conclusion is valid only for an ideal interferometer with no optical losses; the picture changes when these are taken into account.

As in the case of frequency-independent squeezing, we limit ourselves to the analysis of output losses. Using rule (4.8), it is easy to obtain expressions for the total quantum noise spectral density for the pre-filtering setup:

$$S^h_{\rm tot}(\Omega)=\frac{S^h_{\rm SQL}(\Omega)}{2}\left\{\frac{\cosh(2r)-\sinh(2r)\cos(2\theta)+\epsilon^2}{\mathcal{K}(\Omega)}\right.$$
$$\left.-2\sinh(2r)\sin(2\theta)+\mathcal{K}(\Omega)\big[\cosh(2r)+\sinh(2r)\cos(2\theta)\big]\right\}. \tag{4.20}$$

This spectral density reaches its minimum over θ at the same value (4.14) as in the case with no losses:

$$S^h_{\rm tot}(\Omega)=\frac{S^h_{\rm SQL}(\Omega)}{2}\left[\frac{\exp(-2r)+\epsilon^2}{\mathcal{K}(\Omega)}+\mathcal{K}(\Omega)\exp(-2r)\right] \tag{4.21}$$

[cf. Eqn (4.15)].

For the post-filtering setup,

$$S^h_{\rm tot}(\Omega)=\frac{S^h_{\rm SQL}(\Omega)}{2}$$
$$\times\left\{\frac{1}{\mathcal{K}(\Omega)}\left[\exp(-2r)+\exp(2r)\cot^2\zeta+\frac{\epsilon^2}{\sin^2\zeta}\right]\right.$$
$$\left.-2\exp(2r)\cot\zeta+\mathcal{K}(\Omega)\exp(2r)\right\}. \tag{4.22}$$

Here, the presence of losses influences the optimal value of ζ,

$$\cot\zeta(\Omega)=\frac{\mathcal{K}(\Omega)}{1+\epsilon^2\exp(-2r)}\,, \tag{4.23}$$

giving the optimized spectral density

$$S^h_{\rm tot}(\Omega)=\frac{S^h_{\rm SQL}(\Omega)}{2}\left[\frac{\exp(-2r)+\epsilon^2}{\mathcal{K}(\Omega)}+\frac{\epsilon^2\mathcal{K}(\Omega)}{1+\epsilon^2\exp(-2r)}\right]. \tag{4.24}$$

Hence, in the post-filtering setup with the presence of losses, the radiation pressure noise is not fully compensated.

It follows from a comparison of expressions (4.21) and (4.24) that the pre-filtering option becomes preferable when the squeezing is strong or, more precisely, when

$$2\epsilon^2\sinh(2r)>1\,. \tag{4.25}$$

We note that the squeezing of 10 dB ($2\sinh(2r)>10$) was already demonstrated quite a long time ago [82], while it is problematic, at least in second-generation detectors, to decrease the losses to the level of $\epsilon^2<0.1$. Therefore, the pre-filtering setup is probably preferable.

4.2.5 Practical considerations. Another quite serious problem when putting setups with filter cavities together is the optical losses in the cavities themselves. The contribution of these losses to the filter cavity bandwidth should be significantly smaller than the bandwidth itself, i.e.,

$$\frac{cA_{\rm f}}{4L_{\rm f}}\ll\gamma_{\rm f}\,, \tag{4.26}$$

where $L_{\rm f}$ is the filter cavity length and $A_{\rm f}$ is the absorption coefficient per light circulation. Consequently, for typical values $\gamma_{\rm f}\sim10^3$ s^{-1} [see expression (4.29)] and $A_{\rm f}\sim10^{-4}$, the filter cavity length should be at least several tens, or better several hundreds of meters, so as to be comparable to the arm lengths of the gravitational-wave detector itself, which significantly increases its cost.

On the other hand, it was shown in [89, 90] that in considering the real parameters of modern detectors, the combination of two filter cavities is excessive: one is sufficient. Indeed, expression (4.14) (in the pre-filtering case; the same considerations are valid for post-filtering) can be written in the form

$$\tan\theta(\Omega)=\frac{\Omega_{\rm q}^2\gamma^2}{\Omega^2(\gamma^2+\Omega^2)}\,. \tag{4.27}$$

The term Ω^2 in the parentheses in the denominator of (4.27) becomes significant only for $\Omega>\gamma$. On the other hand, in modern detectors $\gamma^2\gg\Omega_{\rm q}^2$, and therefore, for $\Omega>\gamma$, condition (4.27) provides values of θ close to zero. The physical reason for this lies in the fact that for $\Omega>\gamma$, the radiation pressure contribution to the total quantum noise can be disregarded and the squeezing phase $\theta\to0$ becomes optimal and minimizes the shot noise (see the corresponding plot in Fig. 13).

Therefore, Eqn (4.27) can be approximated as

$$\tan\theta(\Omega)=\frac{\Omega_{\rm q}^2}{\Omega^2}\,. \tag{4.28}$$

Using this and (4.19), we can easily obtain the parameters of a single filter cavity that provide such a dependence:

$$\gamma_{\rm f}=\delta_{\rm f}=\Omega_{\rm q}\,. \tag{4.29}$$

Currently, the addition of one short filter cavity (in the pre-filtering case) is very likely to be considered for the upgrade of ALIGO detectors [91, 92]. The length of this cavity, 16 m, is chosen so as to make it possible to install it in the existing ALIGO infrastructure.

4.3 Quantum speed meter

4.3.1 Quantum nondemolition measurements. The principle of quantum nondemolition (QND) measurement was suggested in the 1970s [22, 26] (see also later reviews [93, 94]). This method can be described by the following requirements for a measuring device [95]:

(1) the measuring device should measure an observable Q of the test object such that its operator values at different time moments $\hat{Q}(t)$ (in the Heisenberg representation) commute: $[\hat{Q}(t), \hat{Q}(t')] \equiv 0$. These are called QND observables;

(2) the measuring device should fundamentally not give any information on observables whose operators do not commute with $\hat{Q}$.

If these conditions are satisfied, the values of observables that do not commute with $\hat{Q}$ are, naturally, perturbed, but this does not affect Q itself. Therefore, such systems are free from the SQL.

The mentioned requirements are satisfied by the measurement of an integral of motion of the test object under the condition that the Hamiltonian of its interaction with the measuring device commutes with this observable.[7]

The first 'practical' setups for QND measurements were also proposed in the late 1970s [22–25]. Mainly, they were intended for oscillators, i.e., vibrational modes of the solid-state detectors of that time, with the QND observables chosen as either energy or (in more realistic schemes [23, 24]) the oscillator quadrature amplitude.

A scheme for QND measurements of a free mass was suggested in [25] using its obvious integral of motion, the momentum. Unfortunately, the interaction in this scheme is realized through the magnetic field; a quantum level of sensitivity is hardly attainable in such a scheme due to technological reasons.

4.3.2 Idea of a quantum speed meter. It was proposed in [96] to measure not the momentum but the velocity of the test object by performing two consecutive measurements of its coordinate, such that the quantum state of the speed meter would remain coherent between these measurements and the sign of the interaction would be reversed for the second measurement. Unlike the canonical momentum p, the velocity v and the kinetic momentum mv are not integrals of motion (we recall that if the Hamiltonian of the test object interaction with the measuring device depends on p, the canonical momentum is different from the kinetic one). However, as we see later, if some additional conditions are satisfied, such a scenario allows overcoming the SQL.

The simplest setup of a quantum speed meter is shown in Fig. 16. A light pulse from the laser is first reflected from one side of the test mass and then, after a time delay τ, from the other, and is finally registered with a homodyne detector. It is easy to see that the resulting phase of this pulse can be expressed as

$$\phi_{\text{fin}} = \phi + \frac{2\omega_0\tau}{c}\,\bar{v}\,, \tag{4.30}$$

where ϕ is the initial phase,

$$\bar{v} = \frac{x_\tau - x}{\tau} \tag{4.31}$$

[7] Clearly, the measured observable must respond to the external influence, which needs to be observed, and should therefore be an integral of motion only in the absence of the external influence.

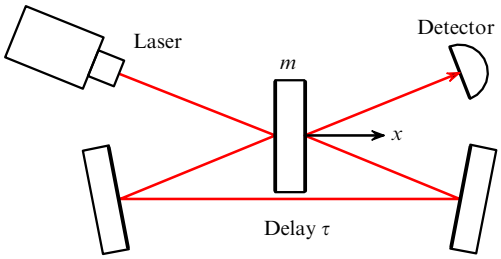

Figure 16. Scheme of a quantum speed meter.

is the mean velocity of the test mass over the time interval between the reflections, and x and x_τ are respective oscillator coordinates at the instants of first and second reflections. The light pulse during the reflection transfers the momentum $2\mathcal{E}/c$ to the test mass, where $\mathcal{E}$ is the energy of the pulse. Therefore, the mean velocity between the reflections is different from the initial velocity v:

$$\bar{v} = v + \frac{2}{mc}\,\mathcal{E}\,; \tag{4.32}$$

hence,

$$\phi_{\text{fin}} = \phi + \frac{2\omega_0\tau}{c}\,v + \frac{4\omega_0\tau}{mc^2}\,\mathcal{E}\,. \tag{4.33}$$

Therefore, when measuring the phase ϕ_{fin}, the accuracy of the initial speed measurement is limited by the value

$$\Delta v = \sqrt{\left(\frac{c\Delta\phi}{2\omega_0\tau}\right)^2 + \left(\frac{2\Delta\mathcal{E}}{mc}\right)^2}\,, \tag{4.34}$$

where $\Delta\phi$ and $\Delta\mathcal{E}$ are initial uncertainties of the light pulse phase and energy. With the uncertainty relation

$$\Delta\mathcal{E}\Delta\phi \geqslant \frac{\hbar\omega_0}{2}\,, \tag{4.35}$$

measurement error (4.34) is limited by the velocity SQL [96]:

$$\Delta v \geqslant \Delta v_{\text{SQL}} = \sqrt{\frac{\hbar}{m\tau}}\,. \tag{4.36}$$

It is obvious, however, that the term proportional to $\mathcal{E}$ in (4.33) can be compensated by measuring not the phase of the light pulse but the linear combination

$$\phi_{\text{fin}} - \frac{4\omega_0\tau}{mc^2}\,\mathcal{E}\,, \tag{4.37}$$

i.e., some optimal quadrature amplitude of the output light. In this case, the measurement error for the initial velocity is

$$\Delta v = \frac{c}{2\omega_0\tau}\,\Delta\phi\,, \tag{4.38}$$

where $\Delta\phi$ is the initial phase uncertainty. It can theoretically be arbitrarily small, which corresponds to a precise measurement of v.

Although the test-object velocity is perturbed during the measurement, this perturbation is compensated after the second reflection of the light pulse:

$$v_{\text{fin}} = \bar{v} - \frac{2}{mc}\,\mathcal{E} = v\,. \tag{4.39}$$

At the same time, the existence of a velocity uncertainty *during the measurement* leads to a random displacement of the object, that is, to the perturbation of its coordinate

$$\Delta x = \frac{2\tau}{mc}\,\Delta\mathcal{E}\,. \tag{4.40}$$

It is easy to see that measurement error (4.38) and perturbation (4.40) satisfy the uncertainty relation

$$\Delta v \Delta x = \frac{\Delta\phi\Delta\mathcal{E}}{\omega_0} \geqslant \frac{\hbar}{2}\,. \tag{4.41}$$

This simple example clearly demonstrates the main features of the quantum speed meter: (a) this measurement is indeed a nondemolition one; (b) in order to achieve an accuracy overcoming the SQL, the measurement (just as the coordinate measurements considered in Section 4.2) requires the introduction of a cross-correlation between the measurement noise and back-action noise.

4.3.3 Sagnac interferometer. The authors of a series of articles [97–103], which followed the original paper [96], suggested several practical schemes for laser gravitational-wave detectors based on the idea of a quantum speed meter with the sensitivity not bounded by the SQL. Here, we consider the version suggested in [101, 102] using the Sagnac interferometer topology. This setup, on the one hand, most accurately follows the initial idea of double coordinate measurement and, on the other hand, is considered one of the most probable candidates for realization in third-generation gravitational-wave detectors.

A simplified schematic of a quantum speed meter based on the Sagnac interferometer is shown in Fig. 17. The light in the arms after reflection from the movable mirror does not return straight to the beam splitter, as in the case of the Michelson interferometer (see Fig. 5), but is first redirected to the other arm and only then recombines on the beam splitter.

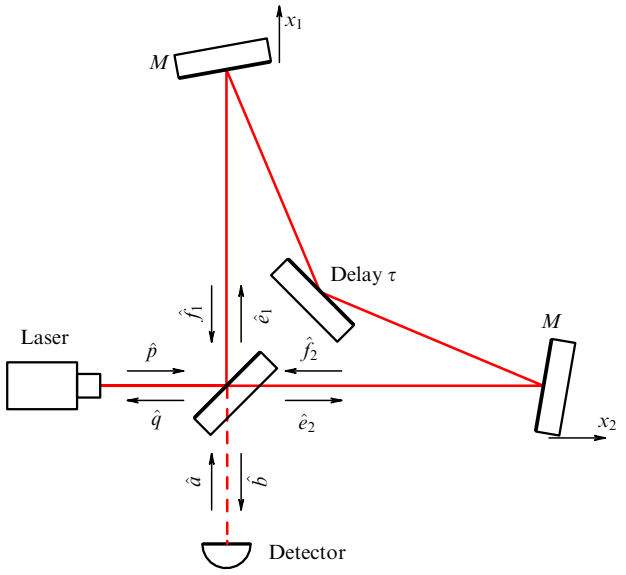

Figure 17. Simplified schematic of a laser gravitational-wave detector based on a quantum speed meter (Sagnac interferometer). *M* are movable mirror masses.

We analyze the operation of this setup following a strategy similar to that in Section 3.1. The quadrature amplitudes of light entering either of the two arms have the same form as in the case of the Michelson interferometer, Eqn (3.8). The light transmitted to the 'northern' arm is first reflected from the 'northern' mirror and then, after a time delay τ, is reflected from the 'eastern' mirror; the light transmitted to the 'eastern' arm follows the same path in the opposite direction. As a result, the quadrature amplitudes of the waves returning to the beam splitter have the form [cf. Eqn (3.10)]

$$\begin{pmatrix}\hat{f}_1^{\,c}(t)\\ \hat{f}_1^{\,s}(t)\end{pmatrix} = \frac{1}{\sqrt{2}}\left\{\begin{pmatrix}P+\hat{p}^{\,c}(t-\tau)\\ \hat{p}^{\,s}(t-\tau)\end{pmatrix} - \begin{pmatrix}\hat{a}^{\,c}(t-\tau)\\ \hat{a}^{\,s}(t-\tau)\end{pmatrix} + \frac{2\omega_0 P}{c}\left(\hat{x}_1(t)+\hat{x}_2(t-\tau)\right)\begin{pmatrix}0\\1\end{pmatrix}\right\}, \tag{4.42a}$$

$$\begin{pmatrix}\hat{f}_2^{\,c}(t)\\ \hat{f}_2^{\,s}(t)\end{pmatrix} = \frac{1}{\sqrt{2}}\left\{\begin{pmatrix}P+\hat{p}^{\,c}(t-\tau)\\ \hat{p}^{\,s}(t-\tau)\end{pmatrix} + \begin{pmatrix}\hat{a}^{\,c}(t-\tau)\\ \hat{a}^{\,s}(t-\tau)\end{pmatrix} + \frac{2\omega_0 P}{c}\left(\hat{x}_2(t)+\hat{x}_1(t-\tau)\right)\begin{pmatrix}0\\1\end{pmatrix}\right\}. \tag{4.42b}$$

For a wave that is directed to the dark port after recombination on the beam splitter, and for the output signal of the homodyne detector, we obtain the respective expressions [see Eqns (3.12) and (3.16)]

$$\begin{pmatrix}\hat{b}_1^{\,c}(t)\\ \hat{b}_1^{\,s}(t)\end{pmatrix} = -\begin{pmatrix}\hat{a}^{\,c}(t-\tau)\\ \hat{a}^{\,s}(t-\tau)\end{pmatrix} + \frac{2\omega_0 P}{c}\left(\hat{x}(t)-\hat{x}(t-\tau)\right)\begin{pmatrix}0\\1\end{pmatrix}, \tag{4.43}$$

$$i_-(t) \propto -\hat{a}^{\,c}(t-\tau)\cos\zeta + \left[-\hat{a}^{\,s}(t-\tau) + \frac{2\omega_0 P}{c}\left(\hat{x}(t)-\hat{x}(t-\tau)\right)\right]\sin\zeta \tag{4.44}$$

[cf. expression (3.17)]. This means that the Sagnac interferometer, similarly to the theoretical scheme discussed above, implements the measurement of the difference between values of $\hat{x}$ at two time instants separated by a time delay τ, i.e., the measurement of the velocity of the differential mechanical mode (3.2) of interferometer test mirrors averaged over the time τ.

We now discuss the back-action noise in this scheme. Here, unlike in the Michelson interferometer, light consequently hits both mirrors while traveling along its circular path in the interferometer:

$$\hat{F}_{\text{fl}\,1}(t) = \sqrt{2}\hbar\omega_0 P\left(\hat{e}_1^{\,c}(t)+\hat{e}_2^{\,c}(t-\tau)\right), \tag{4.45a}$$

$$\hat{F}_{\text{fl}\,2}(t) = \sqrt{2}\hbar\omega_0 P\left(\hat{e}_2^{\,c}(t)+\hat{e}_1^{\,c}(t-\tau)\right). \tag{4.45b}$$

Using Eqns (3.8) and (4.42), we can express the differential force acting on the coordinate $\hat{x}$ as

$$\hat{F}_{\text{fl}}(t) = \hat{F}_{\text{fl}\,1}(t) - \hat{F}_{\text{fl}\,2}(t) = \frac{2\hbar\omega_0 P}{c}\left(\hat{a}^{\,c}(t)-\hat{a}^{\,c}(t-\tau)\right) \tag{4.46}$$

[cf. Eqn (3.26)].

We now rewrite Eqns (4.44) and (4.46) in the spectral representation:

$$i_-(\Omega) \propto \hat{x}(\Omega) + \hat{x}_{\text{fl}}(\Omega)\,, \tag{4.47}$$

where

$$\hat{x}_{\rm fl}(\Omega) = \frac{c}{2\omega_0 P}\,\frac{\hat{a}^{\rm c}(\Omega)\cot\zeta + \hat{a}^{\rm s}(\Omega)}{1-\exp(-{\rm i}\Omega\tau)}\,, \tag{4.48a}$$

$$\hat{F}_{\rm fl}(\Omega) = \frac{2\hbar\omega_0 P}{c}\left[1-\exp({\rm i}\Omega\tau)\right]\hat{a}^{\rm c}(\Omega)\,. \tag{4.48b}$$

Let the time delay be small compared with the characteristic signal variation time Ω^{-1}. Then expressions (4.48) can be simplified:

$$\hat{x}_{\rm fl}(\Omega) = \frac{\hat{v}_{\rm fl}(\Omega)}{-{\rm i}\Omega}\,, \tag{4.49a}$$

$$\hat{F}_{\rm fl}(\Omega) = -{\rm i}\Omega\hat{p}_{\rm fl}(\Omega)\,, \tag{4.49b}$$

where $\hat{v}_{\rm fl}(\Omega)$ and $\hat{p}_{\rm fl}(\Omega)$ are respectively shot noise and radiation pressure noise normalized as the equivalent fluctuation velocity and momentum:

$$\hat{v}_{\rm fl}(\Omega) = -\frac{c}{2\omega_0 P\tau}\left[\hat{a}^{\rm c}(\Omega)\cot\zeta + \hat{a}^{\rm s}(\Omega)\right], \tag{4.50a}$$

$$\hat{p}_{\rm fl}(\Omega) = \frac{2\hbar\omega_0 P\tau}{c}\,\hat{a}^{\rm c}(\Omega)\,. \tag{4.50b}$$

We assume for simplicity that the dark port transmits only zero-point fluctuations (the case with squeezed light injection is considered below). In this case, noise spectral densities (4.49) are expressed as

$$S_x(\Omega) = \frac{S_v}{\Omega^2}\,, \tag{4.51a}$$

$$S_F(\Omega) = \Omega^2 S_p\,, \tag{4.51b}$$

$$S_{xF}(\Omega) = -S_{vp} \tag{4.51c}$$

where

$$S_v = \frac{\hbar c^2}{16\omega_0 I_{\rm c}\tau^2\sin^2\zeta}\,, \tag{4.52a}$$

$$S_p = \frac{4\hbar\omega_0 I_{\rm c}\tau^2}{c^2}\,, \tag{4.52b}$$

$$S_{vp} = -\frac{\hbar}{2}\cot\zeta\,. \tag{4.52c}$$

are *frequency-independent* spectral densities of the $\hat{v}_{\rm fl}$ and $\hat{p}_{\rm fl}$ noises.

We note that spectral densities (4.51a)–(4.51c) satisfy uncertainty condition (2.4) with the exact equality:

$$S_x(\Omega)S_F(\Omega) - S_{xF}^2(\Omega) = S_v S_p - S_{vp}^2 = \frac{\hbar^2}{4}\,. \tag{4.53}$$

The total quantum noise spectral density (2.15) for the interferometer under discussion is

$$S_{\rm tot}^h(\Omega) = \frac{8}{m^2L^2\Omega^2}\left(m^2S_v + 2mS_{vp} + S_p\right). \tag{4.54}$$

In the simplest special case with no cross-correlation of the shot noise or the radiation pressure noise ($\zeta = \pi/2$ and $S_{xF} = 0$), expression (4.54) can be simplified:

$$S_{\rm tot}^h(\Omega) = \frac{8}{mL^2\Omega^2}\left(m^2S_v + S_p\right). \tag{4.55}$$

The obvious optimization of (4.55) with respect to the pump power,

$$\sqrt{\frac{S_p}{S_v}} = \frac{8\omega_0 I_{\rm c}\tau^2}{c^2} = m\,, \tag{4.56}$$

gives

$$S_{\rm tot}^h(\Omega) = S_{\rm SQL}^h(\Omega)\,, \tag{4.57}$$

and hence the sensitivity is in this case limited by the SQL. However, even here the quantum speed meter demonstrates an advantage over the 'conventional' coordinate meter: the total quantum noise spectral density of the latter only touches the SQL at one point, $\Omega = \Omega_{\rm q}$, being higher than the SQL at all other frequencies [see expression (2.27) and Fig. 3]. But for a quantum speed meter, due to a specific frequency dependence of its quantum noises (4.51), the equality $S_{\rm tot}^h = S_{\rm SQL}^h$ holds at all frequencies (taking all the mentioned approximations into account).

The same frequency dependence allows performing full quantum noise optimization (see Section 2.5) for all frequencies without using filter cavities. Indeed, with relation (4.53) taken into account, spectral density (4.54) reaches its minimum with respect to S_{vp} at

$$S_{vp} = -\frac{S_p}{m} \tag{4.58}$$

[cf. Eqn (2.55)], with

$$S_{\rm tot}^h(\Omega) = \frac{2\hbar^2}{L^2\Omega^2 S_p} = \frac{S_{\rm SQL}^h(\Omega)}{2}\,\frac{mc^2}{8\omega_0 I_{\rm c}\tau^2}\,. \tag{4.59}$$

Hence, in principle, the Sagnac interferometer sensitivity is limited only by the available pump power and can be arbitrarily higher than the SQL.

4.3.4 Practical setup of a quantum speed meter. The considered 'simple' Sagnac interferometer has the same main disadvantage as the 'simple' Michelson interferometer: for any reasonable values of the optical power, the resulting optomechanical interaction is too weak. It was suggested in [101, 102] to add Fabry–Perot cavities to the Sagnac interferometer arms, similarly to what was done with the Michelson interferometer. But this results in the technological problem of arranging the 'circular motion' during which the light first enters the cavity in one arm, then in the other arm, and only then returns to the beam splitter. In [101], it was proposed to use orthogonal polarizations of light for these purposes and in [102], to use two opposite propagation directions of light in Fabry–Perot ring cavities. As regards quantum noises, these schemes are equivalent. A simpler version with ring cavities is shown in Fig. 18.

Quantum noises from the Sagnac interferometer with Fabry–Perot cavities in the arms were calculated in [104]. The authors also considered the possibility of injecting 'simple' squeezed light ($\theta = 0$) into the interferometer dark port in order to decrease the required power circulating in the arms. In the notation accepted here, the obtained spectral

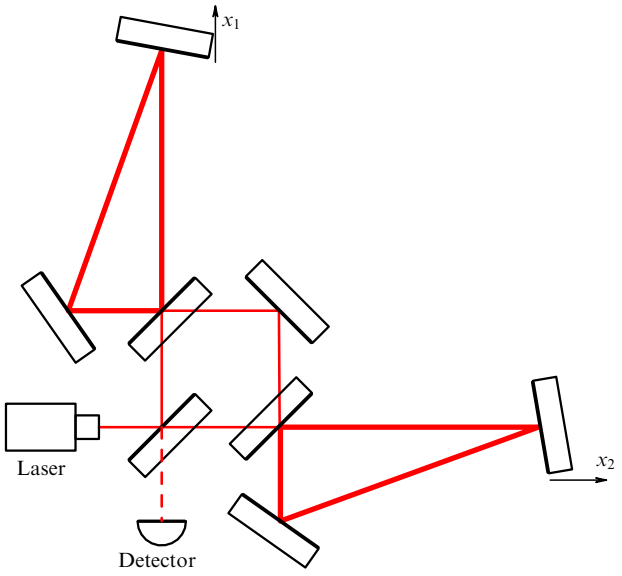

Figure 18. Practical schematic of a laser gravitational-wave detector based on a quantum speedometer (Sagnac interferometer with Fabry–Perot cavities in the arms). The case of triangular cavities in the arms [102]. A setup with conventional linear cavities can be used with additional polarization optics [101].

densities have the form

$$S_v(\Omega) = \frac{\hbar}{2m\mathcal{K}_{\rm SM}(\Omega)}\left[\exp(-2r) + \exp(2r)\cot^2\zeta\right], \quad (4.60a)$$

$$S_p(\Omega) = \frac{\hbar m\mathcal{K}_{\rm SM}(\Omega)}{2}\exp(2r), \quad (4.60b)$$

$$S_{vp} = -\frac{\hbar}{2}\exp(2r)\cot\zeta, \quad (4.60c)$$

where

$$\mathcal{K}_{\rm SM}(\Omega) = \frac{4\Theta\gamma}{m(\gamma^2+\Omega^2)^2} \quad (4.61)$$

is the optomechanical coupling factor for the Fabry–Perot–Sagnac interferometer. Substituting these relations in the expression for the total quantum noise spectral density (4.54), we obtain

$$S^h(\Omega) = \frac{S^h_{\rm SQL}(\Omega)}{2}\left[\frac{\exp(-2r)+\exp(2r)\cot^2\zeta}{\mathcal{K}_{\rm SM}(\Omega)} - 2\exp(2r)\cot\zeta + \mathcal{K}_{\rm SM}(\Omega)\exp(2r)\right]. \quad (4.62)$$

We note that the factor $\mathcal{K}_{\rm SM}(\Omega)$ is radically different from its analogue in the Fabry–Perot–Michelson interferometer, Eqn (3.37), by the fact that $\Omega < \gamma$ inside the Fabry–Perot cavity transmission bands; in other words, in the frequency range where the radiation pressure noise influence is significant, it can be considered approximately independent of the frequency:

$$\mathcal{K}_{\rm SM}(\Omega < \gamma) \approx \mathcal{K}_{\rm SM}(0). \quad (4.63)$$

At $\zeta = \pi/2$ (classical optimization), expression (4.62) takes the form

$$S^h(\Omega) = \frac{S^h_{\rm SQL}(\Omega)}{2}\left[\frac{\exp(-2r)}{\mathcal{K}_{\rm SM}(\Omega)} + \mathcal{K}_{\rm SM}(\Omega)\exp(2r)\right]. \quad (4.64)$$

With (4.63) taken into account, this can be optimized over the whole band $\Omega < \gamma$ by setting

$$\Theta = \frac{m\gamma^3\exp(-2r)}{4}, \quad (4.65)$$

which corresponds to the optimization for a 'simple' Sagnac interferometer in (4.56). Therefore,

$$S^h(\Omega) = \frac{S^h_{\rm SQL}(\Omega)}{2}\left[\frac{\gamma^4}{(\gamma^2+\Omega^2)^2} + \frac{(\gamma^2+\Omega^2)^2}{\gamma^4}\right]. \quad (4.66)$$

It is easy to see that for $\Omega < \gamma$, this spectral density equals the SQL.

We now consider optimizing spectral density (4.62) with respect to the homodyne phase ζ. The existence of Fabry–Perot cavities adds a frequency dependence to spectral densities (4.60), which does not allow performing a frequency-independent optimization similar to (4.58) for all frequencies. However, due to condition (4.63), the following low-frequency optimization becomes possible here:

$$S_{vp} = -\frac{S_p(0)}{m} \;\Rightarrow\; \cot\zeta = \mathcal{K}_{\rm SM}(0) = \frac{4\Theta}{m\gamma^3}. \quad (4.67)$$

Substituting this value of the homodyne phase in expression (4.62), we obtain

$$S^h(\Omega) = \frac{S^h_{\rm SQL}(\Omega)}{2} \times\left[\frac{\exp(-2r)}{\mathcal{K}_{\rm SM}(\Omega)} + \frac{\Omega^4(2\gamma^2+\Omega^2)^2}{\gamma^8}\mathcal{K}_{\rm SM}(\Omega)\exp(2r)\right]. \quad (4.68)$$

It can be seen that for $\Omega < \gamma$, the term proportional to $\mathcal{K}_{\rm SM}$ is suppressed compared with the corresponding term in the case $\zeta = \pi/2$, which allows overcoming the SQL in this frequency range:

$$S^h(\Omega \ll \gamma) = \frac{S^h_{\rm SQL}(\Omega)}{2}\frac{m\gamma^3}{4\Theta}\exp(-2r). \quad (4.69)$$

But if the homodyne phase is not $\pi/2$, it increases the shot-noise contribution, which leads to an increases in S^h at high frequencies.

As was suggested in [105], this problem can be solved by adding a filter cavity (in the post-filtering scheme) to compensate the frequency dependence caused by the finiteness of γ. As was shown in [105], the length and therefore the cost of a filter cavity in such a configuration can be significantly reduced compared with the case of a Fabry–Perot–Michelson interferometer.

Examples of the obtained spectral densities are shown in Fig. 19. We can clearly see that even at $\zeta = \pi/2$ the quantum speed meter scheme may not overcome the SQL, but its sensitivity at low frequencies is significantly higher than in the case of a usual Fabry–Perot–Michelson interferometer (the value of γ for the latter is chosen such that the high-frequency noise has the same level). It is also evident from the figure that there is a slight, but noticeable improvement (an almost two-fold change in the spectral density) in the low-frequency noise level, which can be achieved by using the optimized homodyne phase in (4.67) for the interferometer parameters close to the ALIGO parameters.

4.3.5 Influence of optical losses and a comparison with filter cavity schemes. If optical losses are present in the interferometer output channel, the expression for shot noise in a Fabry–

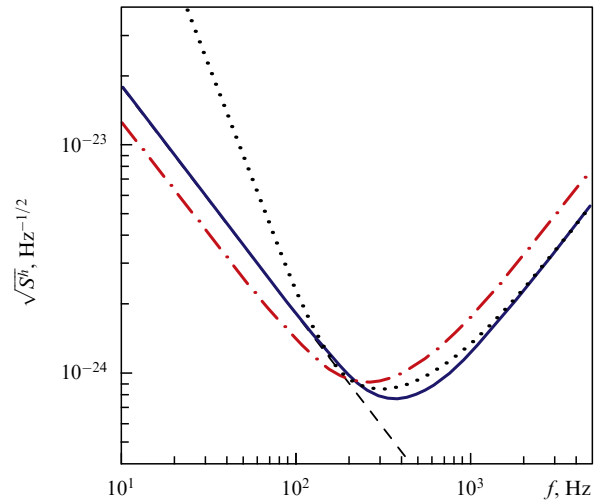

Figure 19. The total quantum noise spectral densities of the Fabry–Perot–Sagnac interferometer at $\zeta = \pi/2$ (solid curve) and for the value of ζ given by (4.67) and providing a minimum of S^h for $\Omega < \gamma$ (dashed-dotted curve). In both cases, γ is determined from (4.65) as $\gamma \approx 2\pi \times 340\ \mathrm{s}^{-1}$. Dotted line: the total quantum noise spectral density of the Fabry–Perot–Michelson interferometer with $\zeta = \pi/2$ and $\gamma = 2\pi \times 680\ \mathrm{s}^{-1}$. For all plots, $\exp(2r) = 10$. Dashed line, the SQL. All parameters not indicated explicitly correspond to ALIGO [see (3.42)].

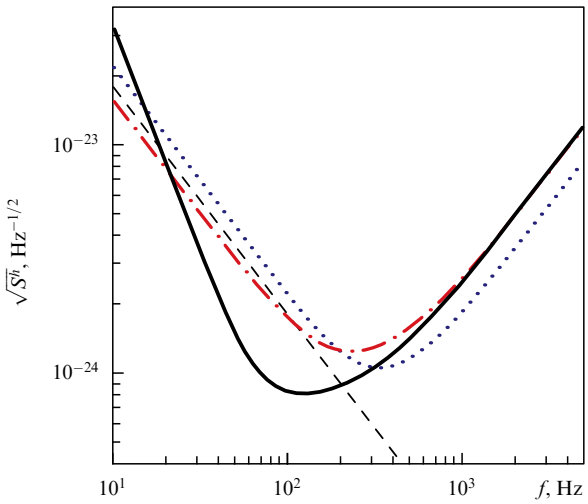

Figure 20. Influence of the optical losses on quantum noise. Solid curve: Fabry–Perot–Michelson interferometer with optimal frequency-dependent squeezing phase (4.14); dotted curve: Fabry–Perot–Sagnac interferometer with $\zeta = \pi/2$; dashed-dotted line: Fabry–Perot–Sagnac interferometer with the optimal ζ, Eqn (4.67). In all plots, $\eta = 0.9$, $\exp(2r) = 10$, and the value of γ is defined by expression (4.71) and is $\approx 2\pi \times 300\ \mathrm{s}^{-1}$. Dashed line: the SQL. All parameters not indicated explicitly correspond to ALIGO [see (3.42)].

Perot–Sagnac interferometer, Eqn (4.60a), becomes [104]

$$S_v(\Omega) = \frac{\hbar}{2m}\,\frac{1}{\mathcal{K}_{\mathrm{SM}}(\Omega)}\left[\exp(-2r) + \exp(2r)\cot^2\zeta + \frac{\epsilon^2}{\sin^2\zeta}\right], \tag{4.70}$$

and spectral densities (4.60b) and (4.60c) stay unchanged.

At $\zeta = \pi/2$ (classical optimization), the total quantum noise spectral density reaches its minimum at

$$\Theta = \frac{m\gamma^3}{4}\sqrt{\exp(-2r)\left[\exp(-2r) + \epsilon^2\right]}, \tag{4.71}$$

with

$$S^h(\Omega) = \frac{S^h_{\mathrm{SQL}}(\Omega)\sqrt{1+\epsilon^2\exp(2r)}}{2} \times \left[\frac{\gamma^4}{(\gamma^2+\Omega^2)^2} + \frac{(\gamma^2+\Omega^2)^2}{\gamma^4}\right] \tag{4.72}$$

[cf. Eqns (4.65) and (4.66)].

Low-frequency optimization with respect to the homodyne phase in the case with losses gives the optimization condition

$$\cot\zeta = \frac{\mathcal{K}_{\mathrm{SM}}(0)}{1+\epsilon^2\exp(-2r)} = \frac{4\Theta}{m\gamma^3\left[1+\epsilon^2\exp(-2r)\right]} \tag{4.73}$$

and the corresponding optimized value of the spectral density

$$S^h(\Omega) = \frac{S^h_{\mathrm{SQL}}(\Omega)}{2}\left\{\frac{\exp(-2r)+\epsilon^2}{\mathcal{K}_{\mathrm{SM}}(\Omega)} + \left[\frac{\Omega^4(2\gamma^2+\Omega^2)^2}{\gamma^8}\exp(2r) + \epsilon^2\right]\frac{\mathcal{K}_{\mathrm{SM}}(\Omega)}{1+\epsilon^2\exp(-2r)}\right\} \tag{4.74}$$

[cf. Eqns (4.67) and (4.68)].

Spectral densities (4.72) and (4.74) are plotted in Fig. 20 together with the corresponding plot for the Fabry–Perot–Michelson interferometer with pre-filtering [see Eqn (4.21)]. In order not to complicate the figure, we do not show the plot for the post-filtering setup because its performance is certainly worse than in the pre-filtering case. As can be seen from Fig. 20, even for quite optimistic values of the unified quantum efficiency $\eta = 0.9$, the losses lead to a noticeable increase in the quantum noise, and the Fabry–Perot–Michelson interferometer scheme with pre-filtering demonstrates the lowest sensitivity to optical losses. On the other hand, due to the specific frequency dependence of the optomechanical coupling factor in the Fabry–Perot–Sagnac interferometer, its sensitivity remains the highest at the lowest frequencies (for the parameter values used in the estimations).

When comparing the prospects of Fabry–Perot–Sagnac interferometers and Fabry–Perot–Michelson interferometers with filter cavities, it is currently difficult to select one best option. Setups with pre- or post-filtering require an additional (expensive) element, a filter cavity. On the other hand, this element is truly additional and does not require a major upgrade of the main interferometer. It can be used for upgrading the existing detectors and detectors under construction.

Regarding future detectors of the so-called third generation, the choice of the best topology will most probably be determined by technological limitations, mainly by the accessible optical power, squeezing, and optical losses. But in any case, the quantum speed meter setup, with its fundamentally different frequency dependence of the quantum noise spectral density at low frequencies (Ω^{-2} instead of Ω^{-4}), is a very promising candidate for realization in such detectors.

Currently, a 'prototype' quantum speed meter based on a Fabry–Perot–Sagnac interferometer is being developed at the University of Glasgow [106, 107].

4.4 Modification of test mass dynamics

4.4.1 Influence of the test mass dynamics on the SQL. In all the setups considered in Sections 4.1–4.3, the sensitivity improvement requires either increasing the optical power circulating in the interferometer or using squeezed light states. We already mentioned the technological problems caused by the high power of the circulating light. The possibility of using squeezed states faces another technological problem, namely, the existence of optical losses in the interferometer, which give rise to vacuum noise and limit the effective squeezing. As a result, we can hope that the considered quantum noise suppression methods can result in improving the sensitivity several-fold or maybe even by an order of magnitude (compared with the ALIGO sensitivity), but its further increase will have to involve some other methods.

One of the proposed alternatives is the enhancement of the signal response of a gravitational-wave detector by modifying the dynamics of its test masses. As can be seen from expressions (2.17) and (2.20), the quantum noises *normalized to the test object input* decrease as the test object susceptibility increases and, as follows from (2.59), the spectral density corresponding to the energetic quantum limit also decreases. Because this does not require any precise mechanisms for mutual compensation of measurement noise and back-action noise (in particular, the SQL does not have to be overcome), the considered method is much more stable with respect to optical losses.

A trivial case of the considered method is just decreasing the test object mass m [see Eqns (2.24) and (2.26)]. Such an approach can be applied, for example, in atomic force microscopes. On the contrary, when detecting forces of a gravitational nature, particularly in gravitational-wave detectors, the signal force is also proportional to the test-object mass; therefore, the overall sensitivity decreases together with the mass, which we can see, for example, from the expressions for the total quantum noise and the SQL in the h-normalization [Eqns (2.27) and (2.28)].

Another possibility is to use a harmonic oscillator instead of a free test mass. The susceptibility of a harmonic oscillator rapidly increases near its resonance frequency $\Omega_{\rm m}$, which improves the SQL by a factor of $\sim \Omega_0/\Delta\Omega$ in the frequency band $\Delta\Omega$ centered at $\Omega_{\rm m}$ [see (2.26) and (2.31)]. This method was demonstrated in several recent 'table-top' experiments with mechanical nano-oscillators [108–110].

In laser gravitational-wave detectors, the characteristic eigenfrequencies of the test mirror vibrational (pendulum) modes are close to 1 Hz, and in the operating frequency range these mirrors can be regarded as almost free masses. Obviously, it is impossible to turn the differential mechanical mode of laser detector test mirrors into an oscillator with a frequency in the operating frequency range by using an 'ordinary' spring. The reason is simply the distance of several hundred meters or several kilometers between these mirrors, not to mention the unacceptable dissipation level and thermal noises introduced by such a spring. However, instead, for the same purposes, one can use the effect of the so-called optical (in a more general context, electromagnetic) rigidity.

4.4.2 Electromagnetic rigidity. This effect was presumably first observed in [111], where the authors investigated a low-frequency torsion pendulum with its coordinate being measured with a radio frequency capacitive sensor. It was observed that the mechanical oscillator eigenfrequency changes with the variation of the pump voltage in the capacitive sensor, and the sign of this change is determined by the sign of the pump frequency detuning from the electromagnetic resonance. This effect was correctly explained in [111] by the dependence of the detuning and hence the energy stored in the capacitive sensor on the mechanical coordinate x.

Indeed, if the eigenfrequency of an electromagnetic resonator depends on x (for small x, this dependence can be approximated linearly),

$$\omega(x) = \omega_0 - gx\,, \tag{4.75}$$

then its detuning is expressed as

$$\delta(x) = \omega_{\rm p} - \omega(x) = \delta + gx\,, \tag{4.76}$$

where $\omega_{\rm p}$ is the pump frequency and δ is the detuning value at $x = 0$. At the same time, the electromagnetic energy stored in the resonator also depends on x:

$$\mathcal{E}(x) = \frac{\gamma^2 + \delta^2}{\gamma^2 + \delta^2(x)}\,\mathcal{E}\,, \tag{4.77}$$

where $\mathcal{E}$ is the energy at $x = 0$. This, in turn, leads to the x-dependence of the ponderomotive force that acts on the mechanical degree of freedom (for example, the electrostatic attraction of capacitor plates in the case of a capacitive sensor or radiation pressure in an optical cavity):

$$F(x) = \frac{g}{\omega_0}\,\mathcal{E}(x)\,. \tag{4.78}$$

The linear component of this dependence gives the electromagnetic rigidity:

$$K = -\left.\frac{\partial F(x)}{\partial x}\right|_{x=0} = \frac{2g^2\mathcal{E}\delta}{\gamma^2 + \delta^2}\,. \tag{4.79}$$

Obviously, when changing x, the energy $\mathcal{E}$ and hence force (4.78) do not change instantly, but with a delay $\tau_{\rm d} \sim 1/\gamma$. Thus, the component of (4.78) proportional to x takes the form

$$-Kx(t - \tau_{\rm d}) \approx -Kx(t) - H\,\frac{{\rm d}x(t)}{{\rm d}t}\,, \tag{4.80}$$

where

$$H = -K\tau_{\rm d} \tag{4.81}$$

is the electromagnetic friction associated with the electromagnetic rigidity.

The existence of this friction allows us to assume that according to the fluctuation–dissipation theorem, the electromagnetic rigidity can be a source of a new fluctuating force that would act on the mechanical object. Indeed, this is the case, but the effective noise temperature of such a force is very low and under certain conditions it can correspond to zero-point fluctuations [112].

Optical rigidity was experimentally demonstrated in small 'table-top' interferometers [113, 114] and in a 40-meter 'prototype' interferometer at the California Institute of Technology [115].

The very low noise temperature of electromagnetic (in particular, optical) rigidity also made it very popular in quantum optomechanical experiments, for example, in the

electromagnetic cooling of mechanical oscillators [116, 117] (see also reviews [28, 29]).

4.4.3 Optical rigidity in laser gravitational-wave detectors. The possibility of using optical rigidity in laser gravitational-wave detectors was first discussed in [118] regarding the topology with the so-called intracavity readout.

The prospects of optical rigidity applications in 'conventional' laser gravitational-wave detectors were considered in [119–122]. The expressions for quantum noises for a detuning δ needed to create optical rigidity are very cumbersome. Therefore, we do not present them here (they can be found, e.g., in [45]) and limit ourselves to an analysis of the test mass dynamics and the SQL value in the presence of optical rigidity.

One of the optical rigidity features is that it is frequency-dependent [120–122]:

$$K(\Omega) = \frac{\Theta\delta}{(\gamma - \mathrm{i}\Omega)^2 + \delta^2} \tag{4.82}$$

[cf. expression (4.79)], and this frequency dependence allows partly compensating the main disadvantage of 'conventional' test oscillators, that is, the narrow band of sensitivity improvement. In the presence of optical rigidity, depending on the interferometer parameters, the SQL

$$S^h_{\mathrm{SQL}}(\Omega) = \hbar\bigl|\chi(\Omega)\bigr|^{-1} = \hbar\bigl|-m\Omega^2 + K(\Omega)\bigr|\,, \tag{4.83}$$

can have either two resonance minima or one broader minimum (the so-called second-order pole regime [120]). If the interferometer bandwidth is sufficiently small, $\gamma \ll \delta$, the frequencies of these minima can be expressed as

$$\Omega^2_{1,2} \approx \left(\frac{\delta^2}{2} \pm \sqrt{\frac{\delta^4}{4} - \frac{\Theta\delta}{m}}\right)^{1/2}, \tag{4.84}$$

and the second-order pole regime is realized for

$$\delta = \left(\frac{4\Theta}{m}\right)^{1/3}. \tag{4.85}$$

The SQL for these two regimes, Eqn (4.83), is shown in Fig. 21. To highlight the effect, we use very small values $\gamma = 2\pi \times 2\ \mathrm{s}^{-1}$. However, such values can be actually applied in configurations with two or more optical pumps, one of which has the 'standard' $\gamma \sim 10^3\ \mathrm{s}^{-1}$ and is used for the measurement, while the other, with the small $\gamma \sim 10\ \mathrm{s}^{-1}$, creates the optical rigidity. The same is valid for the scheme with optical inertia considered in Section 4.4.4, in which up to two additional pumps can be used.

4.4.4 Negative optical inertia. A method for a more thorough modification of the test-mass dynamics was suggested in [123, 124] based on the frequency dependence of optical rigidity in Eqn (4.82).

To demonstrate the principle of this method without complicated calculations, we assume that $\gamma \to 0$ and $\Omega \ll \delta$ in (4.82). In this case,

$$K(\Omega) \approx K(0) - m_{\mathrm{opt}}\Omega^2 + \mathcal{O}(\Omega^4)\,, \tag{4.86}$$

where

$$K(0) = \frac{\Theta}{\delta} \tag{4.87}$$

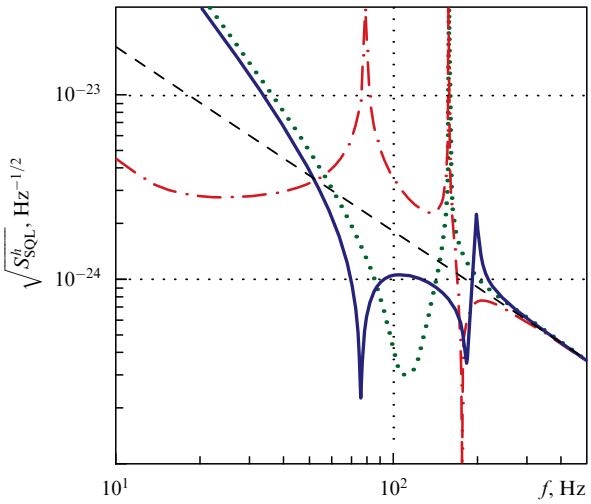

Figure 21. The SQL for a test mass with dynamics modified by optical rigidity. Solid curve: $\gamma = 2\pi \times 2\ \mathrm{s}^{-1}$ and $\delta = 2\pi \times 300\ \mathrm{s}^{-1}$; dotted curve: $\gamma = 2\pi \times 2\ \mathrm{s}^{-1}$ with $\delta \approx 2\pi \times 160\ \mathrm{s}^{-1}$ defined by expression (4.85). Dash-dotted curve: the regime of negative optical inertia: $\gamma_{1,2} = 2\pi \times 2\ \mathrm{s}^{-1}$, $\delta_1 \approx 2\pi \times 80\ \mathrm{s}^{-1}$, $\delta_2 = -2\delta_1$, $I_{\mathrm{c}1}/I_{\mathrm{c}2} = 0.5$, and $I_{\mathrm{c}1} + I_{\mathrm{c}2} = 4 \times 840$ kW [see Eqns (4.90)]. Dashed line: the free-mass SQL. All parameters not indicated explicitly correspond to ALIGO [see (3.42)].

is the static rigidity and

$$m_{\mathrm{opt}} = -\frac{\Theta}{\delta^3} \tag{4.88}$$

is the *effective optical inertia*. We note that depending on the sign of the detuning δ, both these values can be either positive or negative.

We now assume that the interferometer is pumped with two pump lasers having different frequencies. Each pump creates its own optical rigidity. If the detuning of these pump lasers δ_1 and δ_2 have different signs, then the parameters can be combined in such a way that the static rigidities created by the lasers would compensate each other and the introduced total optical inertia would compensate the usual mechanical inertia of the test mass:

$$K_1(0) + K_2(0) = 0\,, \tag{4.89a}$$

$$m + m_{\mathrm{opt}\,1} + m_{\mathrm{opt}\,2} = 0\,. \tag{4.89b}$$

Obviously, the exact compensation takes place only at zero frequency, but at other sufficiently small frequencies, the susceptibility of such a test object would be significantly larger than that of the initial test mass.

More rigorous calculations taking the finiteness of γ into account show that in order to satisfy equalities (4.89), the pump parameters should be such that

$$\Theta_1 = \frac{m(\gamma_1^2 + \delta_1^2)^2(\gamma_2^2 + \delta_2^2)}{\delta_1(\delta_2^2 + \gamma_2^2 - \delta_1^2 - \gamma_1^2)}\,, \tag{4.90a}$$

$$\Theta_2 = \frac{m(\gamma_1^2 + \delta_1^2)(\gamma_2^2 + \delta_2^2)^2}{\delta_2(\delta_1^2 + \gamma_1^2 - \delta_2^2 - \gamma_2^2)}\,. \tag{4.90b}$$

From the plot of the SQL for the negative optical inertia regime in Fig. 21, it is clear (and can also be shown rigorously) that the upper boundary of the range with a decreased SQL corresponds to the lower (in absolute

value) of the two detunings. That detuning, as follows from Eqns (4.90), is defined by the available pump power, $\delta_1 \sim [(\Theta_1 + \Theta_2)/m]^{1/3}$. The 'residual' value $\chi^{-1}(\Omega \to 0) \neq 0$ in this example is created by optical friction: as shown in [123, 124], it can in principle also be compensated by choosing the values of γ for the two pumps.

4.4.5 Setups with intracavity readout. Due to the limited size of this review, we do not consider in detail another class of optical-rigidity-based setups for gravitational-wave detectors, those with the topology of so-called intracavity readout [118, 125–128]. The idea behind these schemes is to couple the motion of test mirrors to the motion of a local mirror (or mirrors) via optical rigidity and measure the position of the local mirror with a small interferometer, instead of directly measuring the positions of the test mirrors separated by a distance of several kilometers.

The described method allows solving one of the main problems of large laser interferometers, namely, the stringent requirements on the circulating optical power. On the other hand, this method requires a radical change in the detector topology, and is currently considered exotic.

5. Conclusions

It is absolutely obvious that the first direct observation of gravitational waves is neither the culmination nor the end of half a century of development of gravitational-wave detectors. The situation is currently as follows: two most advances detectors embodying the best modern technologies could barely 'hear' the signal from a tremendous cosmic catastrophe (during this event, three solar masses were radiated as gravitational waves over fractions of a second) that took place relatively close to us on cosmological scales (at a distance of approximately 0.5 Gpc).

Because gravitational waves from cosmic sources carry a huge amount of astrophysical and physical information, unobtainable with any other method (details can be found in reviews [46, 129, 130]), there is no doubt that the development of more sensitive gravitational-wave detectors will be actively continued.

In the first place, the number of second-generation detectors (ALIGO class) will grow, which would increase the observation reliability for gravitational-wave signals and, importantly, would radically increase the localization accuracy on the celestial sphere. During the next year, the French–Italian detector Advanced Virgo will begin operation [131, 132]. The Kamioka Gravitational Wave Detector (KAGRA) is under construction in Japan [133, 134], which has advanced features such as sapphire test mirrors cooled to 20 K and an underground location, which significantly lowers seismic noises. It has been decided to build a gravitational-wave detector in India using the already developed 'filling', which was initially planned for the third ALIGO detector. There are also plans to build a ground-based gravitational-wave detector in China.

There is little doubt that second-generation detectors will use squeezed light. Most likely, at some later stage of their life cycle, relatively short (several dozen meters) filter cavities will be added to interferometers, probably in the pre-filtering scheme. There are also discussions on the prospects of a more thorough upgrade, comparable to that of the Initial LIGO to ALIGO, which would result in using new mirrors (including cryogenic ones) and suspensions. As a result, the sensitivity of such devices, known as 2.5-generation detectors, should become 2–5 times larger (in the units of the metric h) than the ALIGO sensitivity [58]. We note that the number of registered events will increase as the cube of this factor, i.e., by one to two orders of magnitude.

There are also preliminary projects of third-generation gravitational-wave detectors with a sensitivity one order of magnitude higher than that of ALIGO [44, 135, 136]. They will be able to register gravitational-wave signals from a larger part of the observable Universe for the redshifts up to $z \sim 10$. It is hard to predict which quantum technologies will be used in them. Currently, the most probable candidates are two schemes: either the 'usual' Fabry–Perot–Michelson interferometer with additional long (kilometers) filter cavities or a Fabry–Perot–Sagnac interferometer, possibly with a short filter cavity. However, the experience in using second- and 2.5-generation detectors can change this situation.

In any case, we expect quite interesting results in the next decade both in astrophysics and in the field of quantum measurement technologies.

Acknowledgments

This work was supported by the RFBR grants 14-02-00399 and 16-52-10069 and by the USA NSF grant PHY-1305863.

6. Appendices

A. Spectra and spectral densities

In this review, we let functions of time and their spectra be denoted by the same letter and distinguish them by the explicitly specified argument (time or frequency).

When calculating the spectra, we use the 'quantum-optical' sign rule:

$$f(\Omega) = \int_{-\infty}^{\infty} f(t) \exp(\mathrm{i}\Omega t)\, \mathrm{d}t\,. \tag{A.1}$$

For all spectral densities, except the noise spectral density S^h in the h normalization, we use the 'two-sided' definition:

$$B(t) = \int_{-\infty}^{\infty} S(\Omega) \exp(-\mathrm{i}\Omega t)\, \frac{\mathrm{d}\Omega}{2\pi}\,, \tag{A.2}$$

where $B(t)$ is the corresponding correlation function.

For S^h, following the conventional practice, we use the 'one-sided' definition

$$B^h(t) = \int_0^{\infty} S^h(\Omega) \cos(\Omega t)\, \frac{\mathrm{d}\Omega}{2\pi}\,, \tag{A.3}$$

which gives the following rule for the recalculation from the quantum noise spectral density S^F in the F-normalization to S^h:

$$S^h(\Omega) = \frac{8}{m^2 L^2 \Omega^4}\, S^F(\Omega)\,. \tag{A.4}$$

B. Two-photon formalism

Quadrature amplitudes. In the framework of the two-photon formalism [70, 71], the optical field in a traveling wave can be represented as a superposition of cosine ($\hat{a}^{\mathrm{c}}$) and sine ($\hat{a}^{\mathrm{s}}$) quadrature amplitudes:

$$\hat{a}(t) = \hat{a}^{\mathrm{c}}(t) \cos(\omega_0 t) + \hat{a}^{\mathrm{s}}(t) \sin(\omega_0 t)\,, \tag{B.1}$$

which are operator-valued functions of time that vary slowly on the scale of the frequency ω_0 and satisfy the commutation relations

$$\left[\hat{a}^{\rm c}(t),\hat{a}^{\rm c}(t')\right]=\left[\hat{a}^{\rm s}(t),\hat{a}^{\rm s}(t')\right]=0\,, \tag{B.2a}$$

$$\left[\hat{a}^{\rm c}(t),\hat{a}^{\rm s}(t')\right]={\rm i}\delta(t-t')\,. \tag{B.2b}$$

It follows from commutator (B.2b) that the operator $\hat{a}$ is normalized as a square root of the flux of quanta in an optical wave,

$$\overline{\hat{a}^2(t)}=\frac{\left[\hat{a}^{\rm c}(t)\right]^2+\left[\hat{a}^{\rm s}(t)\right]^2}{2}=\frac{\hat{I}(t)}{\hbar\omega_0}\,, \tag{B.3}$$

where I is the optical power and the bar stands for averaging over a period of time much longer than the optical oscillation period.

If the field has a classical component (mean value), it can be explicitly separated:

$$\hat{a}(t)=\left(A^{\rm c}+\hat{a}^{\rm c}(t)\right)\cos(\omega_0 t)+\left(A^{\rm s}+\hat{a}^{\rm s}(t)\right)\sin(\omega_0 t)\,. \tag{B.4}$$

Obviously, the initial phase can always be chosen in such way that one of these mean values, for example, the sine quadrature, vanishes, which gives

$$\hat{a}(t)=\left(A+\hat{a}^{\rm c}(t)\right)\cos(\omega_0 t)+\hat{a}^{\rm s}(t)\sin(\omega_0 t)\,. \tag{B.5}$$

In this paper, the quadrature amplitude operators are denoted with lowercase letters and the corresponding classical amplitudes with capital letters.

Power and phase fluctuations. In real optomechanical setups, including laser gravitational-wave detectors, in order to ensure significant interaction with the mechanical test object, a large number of optical pump quanta are needed. Therefore, we can assume that

$$\frac{\hat{a}^{\rm c,\,s}}{A}\ll 1\,. \tag{B.6}$$

Hence, ignoring second-order terms, we can represent the optical power as

$$\hat{I}(t)=I+\delta\hat{I}(t)\,, \tag{B.7}$$

where

$$I=\frac{\hbar\omega_0 A^2}{2} \tag{B.8}$$

is the mean power and

$$\delta\hat{I}(t)=\hbar\omega_0 A\hat{a}^{\rm c}(t) \tag{B.9}$$

is its fluctuations. In the same approximation, expression (B.5) can be written in the form

$$\hat{a}(t)=\left(A+\hat{a}^{\rm c}(t)\right)\cos\left(\omega_0 t+\hat{\phi}(t)\right), \tag{B.10}$$

where

$$\hat{\phi}(t)=-\frac{\hat{a}^{\rm s}(t)}{A} \tag{B.11}$$

is the optical wave phase.

Squeezing transformation. In the framework of the two-photon formalism, the transformation of the zero quantum state of light, which is realized by a light-squeezing device, can in general be expressed as

$$\hat{a}^{\rm c}=\hat{z}^{\rm c}\left[\cosh r+\sinh r\cos(2\theta)\right]+\hat{z}^{\rm s}\sinh r\sin(2\theta)\,, \tag{B.12a}$$

$$\hat{a}^{\rm s}=\hat{z}^{\rm s}\left[\cosh r-\sinh r\cos(2\theta)\right]+\hat{z}^{\rm c}\sinh r\sin(2\theta)\,, \tag{B.12b}$$

where $\hat{z}^{\rm c,\,s}$ are quadrature amplitudes corresponding to light in the zero state at the input of the squeezing device. If $\theta=0$, these expressions can be simplified:

$$\hat{a}^{\rm c}=\hat{z}^{\rm c}\exp r\,, \tag{B.13a}$$

$$\hat{a}^{\rm s}=\hat{z}^{\rm s}\exp(-r)\,. \tag{B.13b}$$

Spectral densities. The statistical properties of the quadrature amplitudes are defined by their commutators (B.2). Notably, in the zero quantum state, $\hat{a}^{\rm c}$ and $\hat{a}^{\rm s}$ are two noncorrelated noises with the spectral densities

$$S[\hat{a}^{\rm c}]=S[\hat{a}^{\rm s}]=\frac{1}{2}\,. \tag{B.14}$$

We note that the quantum state of radiation created by an ideal laser, that is, a laser with fully suppressed technological fluctuations, is coherent. It differs from the zero state only by the existence of a mean value $A\neq 0$; therefore, the spectral densities of the quadrature amplitudes are equal to (B.14). By combining (B.14) with (B.9) and (B.11), it is easy to also express the spectral densities of shot fluctuations of the power and phase:

$$S_I=\hbar\omega_0 I\,, \tag{B.15}$$

$$S_\phi=\frac{\hbar\omega_0}{4I}\,. \tag{B.16}$$

In the case of a squeezed state, combining expressions (B.12) and (B.14) yields

$$S[\hat{a}^{\rm c}]=\frac{\cosh(2r)+\sinh(2r)\cos(2\theta)}{2}\,, \tag{B.17a}$$

$$S[\hat{a}^{\rm s}]=\frac{\cosh(2r)-\sinh(2r)\cos(2\theta)}{2}\,, \tag{B.17b}$$

$$S[\hat{a}^{\rm c}\hat{a}^{\rm s}]=\frac{\sinh(2r)\sin(2\theta)}{2}\,, \tag{B.17c}$$

where the last expression defines the quadrature amplitude cross-correlation.

References

1. Abbott B P et al. (LIGO Scientific Collab., Virgo Collab.) *Phys. Rev. Lett.* **116** 061102 (2016)
2. Abbott B P et al. (LIGO Scientific Collab., Virgo Collab.) *Phys. Rev. Lett.* **116** 241103 (2016)
3. Misner Ch W, Thorne K S, Wheeler J A *Gravitation* (San Francisco, Calif.: W. H. Freeman, 1973); Translated into Russian: *Gravitatsiya* Vol. 3 (Moscow: Mir, 1977)
4. Hulse R A *Rev. Mod. Phys.* **66** 699 (1994); *Usp. Fiz. Nauk* **164** 743 (1994)
5. Taylor J H (Jr.) *Rev. Mod. Phys.* **66** 711 (1994); *Usp. Fiz. Nauk* **164** 757 (1994)
6. Blanchet L *Living Rev. Relativity* **17** 2 (2014); http://www.livingreviews.org/lrr-2014-2
7. Will C M *Living Rev. Relativity* **17** 4 (2014); Will C M *Phys. Usp.* **37** 697 (1994); *Usp. Fiz. Nauk* **164** 765 (1994); http://www. livingreviews.org/lrr-2014-4

8. Abbott B P et al. (LIGO Scientific Collab., Virgo Collab.) *Astrophys. J. Lett.* **818** L22 (2016)
9. Lipunov V M et al. *New Astron.* **51** 122 (2017); arXiv:1605.01604; Lipunov V M *Phys. Usp.* **59** (9) (2016) https://doi.org/10.3367/UFNe.2016.03.037759; *Usp. Fiz. Nauk* **186** 1011 (2016); Cherepashchuk A M *Phys. Usp.* **59** (9) (2016) https://doi.org/10.3367/UFNe.2016.03.037819; *Usp. Fiz. Nauk* **186** 1001 (2016)
10. Braginskii V B *Sov. Phys. Usp.* **8** 513 (1966); *Usp. Fiz. Nauk* **86** 433 (1965)
11. Braginskii V B, Rudenko V N *Sov. Phys. Usp.* **13** 165 (1970); *Usp. Fiz. Nauk* **100** 395 (1970)
12. Braginskii V B *Sov. Phys. Usp.* **31** 836 (1988); *Usp. Fiz. Nauk* **156** 93 (1988)
13. Braginskii V B *Phys. Usp.* **43** 691 (2000); *Usp. Fiz. Nauk* **170** 743 (2000)
14. Weber J *Phys. Rev.* **117** 306 (1960)
15. Weber J *Phys. Rev. Lett.* **22** 1320 (1969)
16. Braginskii V B et al. *JETP Lett.* **16** 108 (1972); *Pis'ma Zh. Eksp. Teor. Fiz.* **16** 157 (1972)
17. Michelson P F, Price J C, Taber R C *Science* **237** 150 (1987)
18. Astone P et al. *Phys. Rev. D* **82** 022003 (2010)
19. Kuroda K *Int. J. Mod. Phys. D* **24** 1530032 (2015)
20. Braginskii V B *Sov. Phys. JETP* **26** 831 (1968); *Zh. Eksp. Teor. Fiz.* **53** 1434 (1967)
21. Braginskii V B, Vorontsov Yu I *Sov. Phys. Usp.* **18** 644 (1975); *Usp. Fiz. Nauk* **114** 41 (1974)
22. Braginskii V B, Vorontsov Yu I, Khalili F Ya *Sov. Phys. JETP* **46** 705 (1977); *Zh. Eksp. Teor. Fiz.* **73** 1340 (1977)
23. Braginskii V B, Vorontsov Yu I, Khalili F Ya *JETP Lett.* **27** 276 (1978); *Pis'ma Zh. Eksp. Teor. Fiz.* **27** 296 (1978)
24. Thorne K S et al. *Phys. Rev. Lett.* **40** 667 (1978)
25. Caves C M et al. *Rev. Mod. Phys.* **52** 341 (1980)
26. Braginsky V B, Vorontsov Y I, Thorne K S *Science* **209** 547 (1980)
27. Gertsenshtein M E, Pustovoit V I *Sov. Phys. JETP* **16** 433 (1963); *Zh. Eksp. Teor. Fiz.* **43** 605 (1962)
28. Aspelmeyer M, Kippenberg T J, Marquardt F *Rev. Mod. Phys.* **86** 1391 (2014)
29. Khalili F Ya, Danilishin S L *Prog. Opt.* **61** 113 (2016)
30. Wollman E E et al. *Science* **349** 952 (2015)
31. Moss G E, Miller L R, Forward R L *Appl. Opt.* **10** 2495 (1971)
32. Shoemaker D et al. *Phys. Rev. D* **38** 423 (1988)
33. Robertson D I et al. *Rev. Sci. Instrum.* **66** 4447 (1995)
34. Abramovici A et al. *Phys. Lett. A* **218** 157 (1996)
35. Abramovici A et al. *Science* **256** 325 (1992)
36. LIGO: Laser Interferometer Gravitational-Wave Observatory, http://www.ligo.caltech.edu
37. VIRGO interferometer, http://www.virgo.infn.it/
38. GEO600: Gravitational Wave Detector, http://www.geo600.org
39. Gravitational Wave Project Office, National Astronomical Observatory of Japan, http://gwpo.nao.ac.jp/en/
40. Abbott B P et al. *Rep. Prog. Phys.* **72** 076901 (2009)
41. Caves C M *Phys. Rev. D* **23** 1693 (1981)
42. Aasi J et al. *Nature Photon.* **7** 613 (2013)
43. Aasi J et al. *Class. Quantum Grav.* **32** 074001 (2015)
44. Sathyaprakash B et al. *Class. Quantum Grav.* **29** 124013 (2012)
45. Danilishin S L, Khalili F Ya *Living Rev. Relativity* **15** 5 (2012); http://www.livingreviews.org/lrr-2012-5
46. Sathyaprakash B S, Schutz B F *Living Rev. Relativity* **12** 2 (2009); http://www.livingreviews.org/lrr-2009-2
47. Vorontsov Yu I, Khalili F Ya *Radiotekh. Elektron.* **27** 2392 (1982)
48. Braginsky V B, Khalili F Ya *Quantum Measurement* (Cambridge: Cambridge Univ. Press, 1992) Ch. VI
49. Braginsky V B et al. *Phys. Rev. D* **67** 082001 (2003)
50. Braginskii V B, Nazarenko V S *Sov. Phys. JETP* **30** 770 (1970); *Zh. Eksp. Teor. Fiz.* **57** 1421 (1969)
51. O'Connell A D et al. *Nature* **464** 697 (2010)
52. Saulson P R *Phys. Rev. D* **42** 2437 (1990)
53. Zurek W, in *Frontiers of Nonequilibrium Statistical Physics* (Eds G T Moore, M O Scully) (New York: Plenum Press, 1986) p. 145
54. Zurek W H *Rev. Mod. Phys.* **75** 715 (2003)
55. Braginskii V B, Mitrofanov V P, Tokmakov K V *Bull. Russ. Acad. Sci. Phys.* **64** 1333 (2000); *Izv. Ross. Akad. Nauk Ser. Fiz.* **64** 1671 (2000)
56. Braginsky V B, Gorodetsky M L, Vyatchanin S P "Compendium of thermal noises in optical mirrors", in *Optical Coatings and Thermal Noise in Precision Measurement* (Eds G Harry, T P Bodiya, R DeSalvo) (Cambridge: Cambridge Univ. Press, 2012) Ch. 3
57. Ballmer S, Mandic V *Annu. Rev. Nucl. Part. Sci.* **65** 555 (2015)
58. McClelland D et al. (LIGO Scientific Collab.) "Instrument science white paper 2015", LIGO Document T1500290; https://dcc.ligo.org/LIGO-T1500290/public
59. Unruh W G "Quantum noise in the interferometer detector", in *Quantum Optics, Experimental Gravity, and Measurement Theory* (NATO Advanced Science Institutes Series, Ser. B, Vol. 94, Eds P Meystre, M O Scully) (New York: Plenum Press, 1983) p. 647
60. Khalili F Ya *Sov. Phys. Dokl.* **32** 409 (1987); *Dokl. Akad. Nauk SSSR* **294** 602 (1987)
61. Braginsky V B, Khalili F Ya *Quantum Measurement* (Cambridge: Cambridge Univ. Press, 1992) Ch. VIII
62. Jaekel M T, Reynaud S *Europhys. Lett.* **13** 301 (1990)
63. Khalili F Ya *Vestn. Mosk. Gos. Univ. Ser. 3 Fiz. Astron.* **24** 17 (1983)
64. Vorontsov Yu I, Khalili F Ya *Vestn. Mosk. Gos. Univ. Ser. 3 Fiz. Astron.* **26** (3) 3 (1985)
65. Braginsky V B, Khalili F Ya *Quantum Measurement* (Cambridge: Cambridge Univ. Press, 1992) Ch. IX
66. Braginsky V B, Gorodetsky M L, Khalili F Ya, Thorne K S *AIP Conf. Proc.* **523** 180 (2000)
67. Braginsky V B, Strigin S E, Vyatchanin S P *Phys. Lett. A* **287** 331 (2001)
68. Vyatchanin S P, Strigin S E *Phys. Usp.* **55** 1115 (2012); *Usp. Fiz. Nauk* **182** 1195 (2012)
69. Evans M et al. *Phys. Rev. Lett.* **114** 161102 (2015)
70. Caves C M, Schumaker B L *Phys. Rev. A* **31** 3068 (1985)
71. Schumaker B L, Caves C M *Phys. Rev. A* **31** 3093 (1985)
72. LIGO: Look Deeper, https://www.ligo.caltech.edu/page/look-deeper
73. Drever R W P *Lecture Notes Phys.* **124** 321 (1983)
74. Meers B J *Phys. Rev. D* **38** 2317 (1988)
75. Kondrashov I S, Simakov D A, Khalili F Ya, Danilishin S L *Phys. Rev. D* **78** 062004 (2008)
76. Mizuno J et al. *Phys. Lett. A* **175** 273 (1993)
77. Kimble H J et al. *Phys. Rev. D* **65** 022002 (2001)
78. Takahasi H *Adv. Commun. Syst.* **1** 227 (1965)
79. Schleich W P *Quantum Optics in Phase Space* (Berlin: Wiley-VCH, 2001); Translated into Russian: *Kvantovaya Optika v Fazovom Prostranstve* (Moscow: Fizmatlit, 2005)
80. Slusher R E et al. *Phys. Rev. Lett.* **55** 2409 (1985)
81. McKenzie K et al. *Phys. Rev. Lett.* **93** 161105 (2004)
82. Vahlbruch H et al. *Phys. Rev. Lett.* **97** 011101 (2006)
83. Vahlbruch H et al. *Phys. Rev. Lett.* **100** 033602 (2008)
84. Abadie J et al. (The LIGO Scientific Collab.) *Nature Phys.* **7** 962 (2011)
85. Grote H et al. *Phys. Rev. Lett.* **110** 181101 (2013)
86. Vyatchanin S P, Matsko A B *JETP* **77** 218 (1993); *Zh. Eksp. Teor. Fiz.* **104** 2668 (1993)
87. Vyatchanin S P, Zubova E A, Matsko A B *Opt. Commun.* **109** 492 (1994)
88. Vyatchanin S P, Zubova E A *Phys. Lett. A* **201** 269 (1995)
89. Khalili F Ya *Phys. Rev. D* **76** 102002 (2007)
90. Khalili F Ya *Phys. Rev. D* **81** 122002 (2010)
91. Evans M et al. *Phys. Rev. D* **88** 022002 (2013)
92. Kwee P et al. *Phys. Rev. D* **90** 062006 (2014)
93. Vorontsov Yu I *Phys. Usp.* **37** 81 (1994); *Usp. Fiz. Nauk* **164** 89 (1994)
94. Braginsky V B, Khalili F Ya *Rev. Mod. Phys.* **68** 1 (1996)
95. Braginsky V B, Khalili F Ya *Quantum Measurement* (Cambridge: Cambridge Univ. Press, 1992) Ch. V
96. Braginsky V B, Khalili F Ja *Phys. Lett. A* **147** 251 (1990)
97. Khalili F Ya, Levin Yu *Phys. Rev. D* **54** 4735 (1996)
98. Braginsky V B, Gorodetsky M L, Khalili F Ya, Thorne K S *Phys. Rev. D* **61** 044002 (2000)
99. Purdue P *Phys. Rev. D* **66** 022001 (2002)
100. Purdue P, Chen Y *Phys. Rev. D* **66** 122004 (2002)
101. Khalili F Ya, gr-qc/0211088
102. Chen Y *Phys. Rev. D* **67** 122004 (2003)
103. Danilishin S L *Phys. Rev. D* **69** 102003 (2004)

104. Chen Y et al. *Gen. Relat. Grav.* **43** 671 (2011)
105. Voronchev N V, Tarabrin S P, Danilishin S L, arXiv:1503.01062
106. Gräf C et al. *Class. Quant. Grav.* **31** 215009 (2014)
107. Danilishin S L et al. *New J. Phys.* **17** 043031 (2015)
108. Teufel J D et al. *Nature Nanotechnol.* **4** 820 (2009)
109. Anetsberger G et al. *Nature Phys.* **5** 909 (2009)
110. Westphal T et al. *Phys. Rev. A* **85** 063806 (2012)
111. Braginsky V B, Minakova I I *Vestn. Mosk. Gos. Univ. Ser. 3 Fiz. Astron.* (1) 83 (1964)
112. Braginsky V B, Khalili F Ya *Phys. Lett. A* **257** 241 (1999)
113. Bilenko I A, Samoilenko A A *Vestn. Mosk. Gos. Univ. Ser. 3 Fiz. Astron.* (4) 39 (2003)
114. Corbitt T et al. *Phys. Rev. Lett.* **98** 150802 (2007)
115. Miyakawa O et al. *Phys. Rev. D* **74** 022001 (2006)
116. Teufel J D et al. *Nature* **475** 359 (2011)
117. Chan J et al. *Nature* **478** 89 (2011)
118. Braginsky V B, Gorodetsky M L, Khalili F Ya *Phys. Lett. A* **232** 340 (1997)
119. Buonanno A, Chen Y *Phys. Rev. D* **64** 042006 (2001)
120. Khalili F Ya *Phys. Lett. A* **288** 251 (2001)
121. Buonanno A, Chen Y *Phys. Rev. D* **65** 042001 (2002)
122. Buonanno A, Chen Y *Phys. Rev. D* **67** 062002 (2003)
123. Khalili F et al. *Phys. Rev. D* **83** 062003 (2011)
124. Voronchev N V, Danilishin S L, Khalili F Ya *Opt. Spectrosc.* **112** 377 (2012); *Opt. Spektrosk.* **112** 418 (2012)
125. Braginsky V B, Gorodetsky M L, Khalili F Ya *Phys. Lett. A* **246** 485 (1998)
126. Khalili F Ya *Phys. Lett. A* **298** 308 (2002)
127. Danilishin S L, Khalili F Ya *Phys. Rev. D* **73** 022002 (2006)
128. Rehbein H et al. *Phys. Rev. D* **76** 062002 (2007)
129. Grishchuk L P et al. *Phys. Usp.* **44** 1 (2001); *Usp. Fiz. Nauk* **171** 3 (2001)
130. Scheel M A, Thorne K S *Phys. Usp.* **57** 342 (2014); *Usp. Fiz. Nauk* **184** 367 (2014)
131. Acernese F et al. *Class. Quant. Grav.* **32** 024001 (2015)
132. Advanced Virgo, http://www.virgo-gw.eu/advirgo/
133. Aso Y et al. (The KAGRA Collab.) *Phys. Rev. D* **88** 043007 (2013)
134. KAGRA, http://gwcenter.icrr.u-tokyo.ac.jp/en/
135. Hild S et al. *Class. Quantum Grav.* **28** 094013 (2011)
136. Dwyer S et al. *Phys. Rev. D* **91** 082001 (2015)